Ultra High Temperature Ceramics for Hypersonic Vehicle Applications

Ronald Loehman, Erica Corral, Hans Peter Dumm, Paul Kotula, and Rajan Tandon

Sandia National Laboratories

Ultra High Temperature Ceramics for Hypersonic Vehicle Applications

Ronald Loehman[1], Erica Corral[1], Hans Peter Dumm[1], Paul Kotula[2], and Raj Tandon[3]

[1]Ceramic Processing and Inorganic Materials Department, [2]Materials Characterization Department, [3]Materials Reliability Department

Sandia National Laboratories
P.O. Box 5800
Albuquerque, New Mexico 87185-MS1349

Abstract

HfB_2 and ZrB_2 are of interest for thermal protection materials because of favorable thermal stability, mechanical properties, and oxidation resistance. We have made dense diboride ceramics with 2 to 20 % SiC by hot pressing at 2000°C and 5000 psi. High-resolution transmission electron microscopy (TEM) shows very thin grain boundary phases that suggest liquid phase sintering. Fracture toughness measurements give RT values of 4 to 6 $MPam^{1/2}$. Four-pt flexure strengths measured in air up to 1450°C were as high as 450 – 500 MPa. Thermal diffusivities were measured to 2000°C for ZrB_2 and HfB_2 ceramics with SiC contents from 2 to 20%. Thermal conductivities were calculated from thermal diffusivities and measured heat capacities. Thermal diffusivities were modeled using different two-phase composite models. These materials exhibit excellent high temperature properties and are attractive for further development for thermal protection systems.

ACKNOWLEDGMENTS

CONTENTS

FIGURES

TABLES

Nomenclature

α	thermal diffusivity
CTE	coefficient of thermal expansion
C_p	heat capacity SEM scanning electron microscopy
κ	thermal conductivity
TEM	transmission electron microscopy
UHTC	ultrahigh temperature ceramics

Introduction

Reentry vehicles, regardless of their specific designs, require control surfaces with sharp leading edges if they are to be maneuverable at hypersonic velocities. Low-radius leading edges are subject to much greater aerothermal heating than blunt edges, such as those on the Space Shuttle, and they thus will reach temperatures that may exceed 2000°C during reentry. Available thermal protection materials will not survive such extreme temperatures and new materials are required for advanced thermal protection systems.

The goal of this three year project, which started in October, 2002, was to develop thermal protection materials based on zirconium and hafnium diborides that are more heat and oxidation resistant than materials presently available. Those diboride compounds and composites in which they are the primary constituent are referred to as ultra high temperature ceramics (UHTCs) because they have some of the highest melting points known, above 3200°C. Previous attempts to make these UHTCs had shown mixed results and the properties obtained were inconsistent. Achieving that goal required gaining an understanding of the performance-limiting features of the UHTC specimens and using that understanding to make better thermal protection materials based on Zr and Hf diborides.

 The specific objectives of this project were to:
• Develop improved processing for HfB_2 - and ZrB_2 - based UHTCs
• Develop a data base of reliable UHTC physical and mechanical properties
• Determine the relation between UHTC microstructure and properties using advanced electron microscopic analysis
• Determine the origin and type of failure for UHTCs subjected to realistic stresses and feed back that information to improve processing

Background

Hafnium diboride (HfB_2) and zirconium diboride (ZrB_2) are two ultra high temperature ceramics (UHTCs) with melting points above 3000°C. They are candidates for thermal protection materials in both reentry and hypersonic vehicles because of their high melting points and good oxidation resistance[1,2,3,4]. Their high melting points and oxidation resistance may allow more advanced vehicle designs with features like sharp leading edges and sharp nosecones. Such design features could produce more agile vehicles that would open up a greater range of hypersonic flight paths and reentry trajectories[4].

The lack of economical processing methods has limited the application of the diboride UHTCs. The earliest comprehensive literature reports on Zr and Hf diborides resulted from U.S. Air Force contracts to Manlabs, Inc. in the late 1960's and early 1970's.[2] Kaufman and Clougherty conducted an extensive study of the properties of what were the best HfB_2 and ZrB_2 available at that time. They prepared single crystals by floating zone refining and polycrystalline material by high-pressure hot pressing. They measured properties such as lattice parameters, x-ray thermal expansion, linear thermal expansion,

electrical resistivity and micro hardness of those materials. They also reported that additions of silicon carbide to the pure diborides increased their oxidation resistance.[2]

Upadhya, et al.[5] discussed the advantages of the high melting points and relatively low vapor pressures of HfO_2 and ZrO_2 compared to other oxides. The properties of these oxides are of interest because they are the products of HfB_2 and ZrB_2 oxidation. Upadhya, et al.[5] observed that the large volume change due to the solid-phase transformations of these oxides (monoclinic to tetragonal at 1150° and 1650°C and from tetragonal to cubic at 2370° and 2700°C, for ZrO_2 and HfO_2, respectively) could result in destruction of any large-scale component made from them. Therefore, for practical applications HfB_2 and ZrB_2 must contain appropriate additives so the oxides that form on them will be phase-stabilized to avoid destructive phase transformations.

The kinetics of high temperature oxidation of ZrB_2 were studied by Kuriakose and Margrave[37] and Tripp, et al.[38] High temperature oxidation of zone melted HfB_2 and ZrB_2 was investigated by Berkowitz-Mattuck[8]. Tripp, et al.[14] studied the role of added SiC in the formation of an oxygen diffusion barrier on ZrB_2 between 800°and 1500°C. Oxidation behavior of ZrB_2 powders below 800°C was reported recently by Zheng, et al.[10] Bargeron, et al.[39] studied mechanisms of HfB_2 oxidation in the temperature range of 1400 to 2100°C. Recently Zhang, et al.[9] reported the reactive hot pressing of ZrB_2-SiC composites.

Phase Behavior: Zr and Hf diborides prepared by powder-metallurgy techniques were found to form more than one boride phase. Some of these phases show extended homogeneity ranges, and some have limited temperature ranges of stability[1, 2]. Very high melting temperatures, slow solid-state reaction rates and boron vaporization are the three key factors that complicated the determination of accurate phase equilibrium diagrams for HfB_2 and ZrB_2[2]. The very high liquidus temperatures of these transition metal-boron systems prohibit conventional thermal analysis, which resulted in the availability of little experimental data for the very high temperature regions of the phase diagrams. Difficult to detect invariant reactions or errors in the determination of the range of temperature for a detectable reaction make it difficult to assess the true temperature range of stability of any intermediate phases in these systems[2]. Boron vaporization at high temperatures may lead to the formation of new phases on the surface that can have equilibrium properties that are not characteristic of entire sample. Therefore the true temperature ranges of intermediate phases for Hf-B and Zr-B systems have been difficult to determine.

Figures 1 and 2a are the phase diagrams for Hf-B and Zr-B systems reported by McHale[36]. The diagrams show that the two important compounds formed in the Hf-B system are the monoboride and diboride. Hafnium diboride has a melting temperature of 3380°C with a narrow range of homogeneity as indicated by the lack of significant change of lattice parameters with change in composition[5]. Figure 1 predicts that compositions deficient in boron will contain HfB and HfB_2. For preparations less than 66.7% boron, a FCC phase identified as HfB was detected[17]. Some studies suggest that there are two different hafnium monoborides, one with a cubic structure and the other with an orthorhombic structure, whereas hafnium diboride has a hexagonal crystal

structure[2]. Hafnium monoboride with the FeB structure is a stable phase[2]. Figure 1 is in excellent agreement with the phase behavior reported by E. Rudy et al.[41].
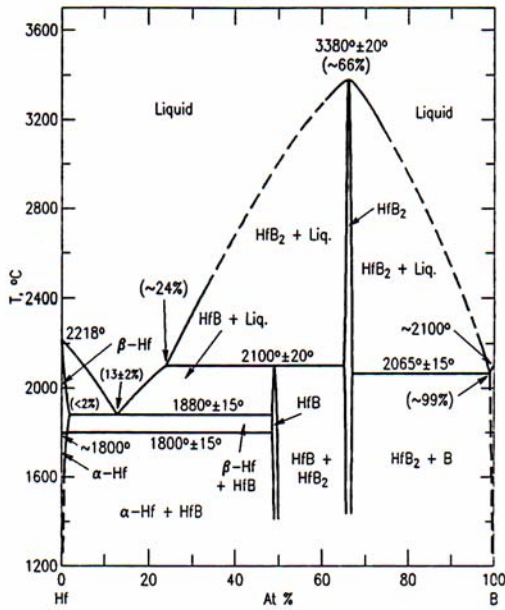
Figure 1. Hf-B system [36]
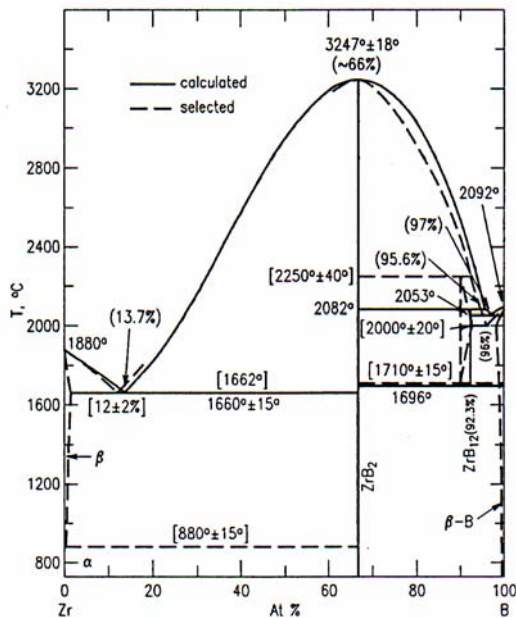
Figure 2a. Zr-B system[36]

10
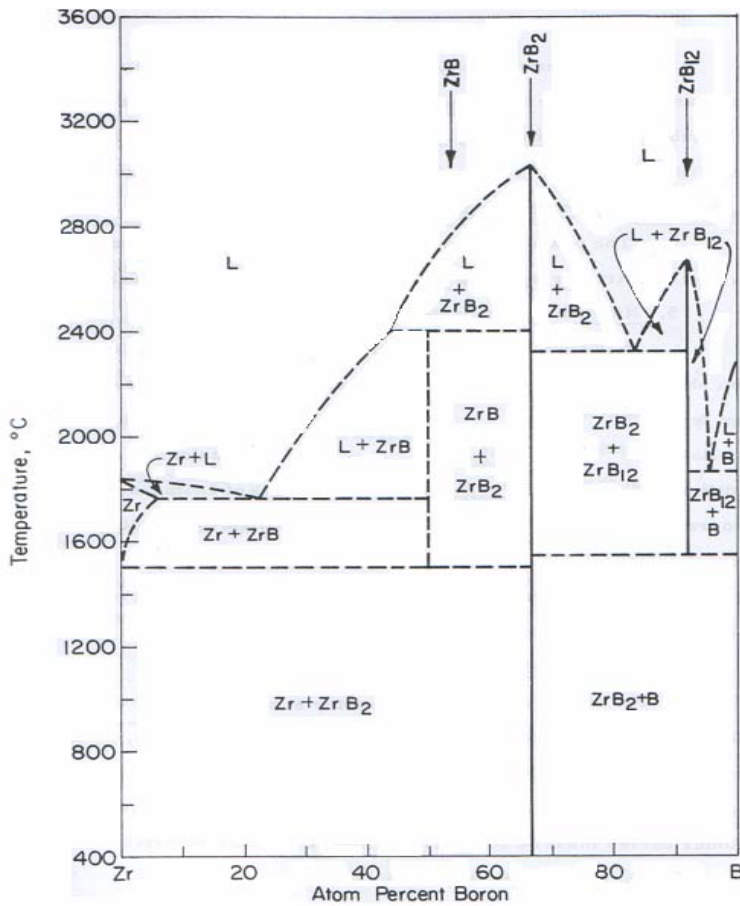
Figure 2b. Zr-B system[2]

ZrB$_2$ is the dominant phase in the zirconium-boron system with a melting point of 3247°C. Schedler's phase diagram of the Zr-B system, as reported by Kaufman[2], shows a ZrB phase (Figure 2b). The diagram also shows that a ZrB$_{12}$ phase exists between 1700°C and 2680°C. From Figure 2a it is evident that the solidus temperature of ZrB$_{12}$ is 2250°C and that ZrB$_{12}$ has a peritectic decomposition, whereas Figure 2b depicts a eutectic mixture of ZrB$_2$ and ZrB$_{12}$ with a eutectic temperature of approximately 2300°C. Figure 2a agrees with the values obtained by Rudy, et al.[41]. Figure 2a also accords with the investigation of solidus temperature of ZrB$_2$ by Rudy, et al., and other reports, whereas Figure 2b suggests a value of 3000° C, which is 400°C less than the melting point of ZrB$_2$. According to Aronsson[18], in cases where ZrB has been observed, considerable O, C or N might have been present to stabilize the cubic structure, which is generally assumed to be the ZrB phase. The ZrB$_2$ phase is shown to have a very limited range of homogeneity and, as predicted by the phase diagram in Figure 2a, off-stoichiometry compounds will contain either free boron or zirconium below 1500° C and may contain ZrB and ZrB$_{12}$ in the range of 1500° to 2200° C. Table 1 summarizes the intermediate phases in the hafnium-boron and zirconium-boron systems.

Table 1. Intermediate Phases in the
Hafnium-Boron and Zirconium-Boron Systems[2, 40]

Phase	Crystal Structure	Crystal Parameters ($A°$)
HfB	Cubic (B1)	a = 4.62
	Orthorhombic (B27)	a = 6.50, b = 3.21, c = 4.82
HfB_2	Hexagonal (C32)	a = 3.141, c = 3.470
ZrB	Cubic (B1)	a = 3.170, c = 3.533
	Orthorhombic (B27)	(None Reported)
ZrB_2	Hexagonal (C32)	a = 3.170, c = 3.533
ZrB_{12}	Cubic (B1)	a = 7.408

Oxidation Behavior: Oxidation of hafnium diboride forms gaseous products at the interface, creating voids and easy oxygen access. As studied by Metcalfe, et al.[11] and many others, the products of oxidation are hafnium dioxide (HfO_2) and boric oxide (B_2O_3). When the system is below the boiling point of B_2O_3 (1500°C at 1 atm pressure) the oxidation resistance of HfB_2 increases due to the sealing of voids in the hafnium by liquid B_2O_3. Additions of HfC to HfB_2 under these conditions degrade the oxidation resistance by generating porosity. At temperatures above 1600°C and lower system pressures (above the boiling point of B_2O_3) the oxidation resistance of HfB_2 is poor. Under these conditions HfC additions to HfB_2 reduce the disruption of the protective surface layer because continuous formation of CO keeps the oxide sufficiently porous to allow the B_2O_3 to escape with much less damage to the HfO_2 films. The addition of SiC to HfB_2 enhances oxidation resistance by two mechanisms. The first is similar to that for HfC additions: continuous evolution of CO keeps the HfO_2 porous and permits non-destructive escape of the B_2O_3 gas. The second mechanism involves the generation of a borosilicate melt that reduces the destructive effect of boiling by continuously replenishing the protective layer it forms as it oxidizes.

Parabolic rate constants were obtained in a study of oxidation of zone melted HfB_2 by Berkowitz-Mattuck[8] at temperatures between 1488 and 2000 K and oxygen partial pressures of 8.5 and 19.9 torr. Oxidation of Man Labs HfB_2 (high pressure hot pressed, pycnometric density 10.74 g/cm^{3}, and 97.9% of theoretical) at 2024 - 1982 K with oxygen partial pressure of 18.5 torr and a carrier gas flow rate of 119 cm[3]/min gave parabolic rate constants. These studies of oxidation of HfB_2 predicted superior oxidation resistance of the metal-rich diboride[2]. Oxidation mechanisms of HfB_2 studied by Bargeron et al.[39] suggest that gaseous products form at the interface and create voids that allow easy oxygen access. They[39] also point out that a phase transition occurs in hafnium dioxide at approximately 1700°C, which can result in cracking due to volume change.

The overall conclusion of these studies is that oxygen does not dissolve into bulk HfB_2 during oxidation of HfB_2, and that gaseous products will be present at temperatures near and above the boiling point of B_2O_3.

ZrB_2 resists oxidation up to temperatures of 1000°-1300°C. The oxidation rate of ZrB_2 at temperatures of 1218 – 1529 K and oxygen pressures between 100 and 760 torr, as determined by Kuriakose and Margrave[37], fit to a parabolic rate law and was independent of carrier gas flow rate and was directly proportional to the oxygen partial pressure in helium. Metallographic examination of the oxide scale formed on ZrB_2 at 1000°C led Meyerson and Samsonov[2, 16] to postulate that a sub-stoichiometric $ZrO_2(s)$ exists at the alloy-oxide interface. They suggested that such a film of ZrO_2 covered by fluid B_2O_3 (possibly containing dissolved ZrO_2) is initially formed on the surface of the ZrB_2 in the first 2 hours in oxygen at 1000°C and that oxygen diffuses through the oxide and reacts with the sub-stoichiometric ZrO_2 to form ZrO_2 for longer heating times. During heating the B_2O_3 gradually evaporates.

Zheng, et al.[10] suggested that oxidation of ZrB_2 powder below 1073 K in air occurs according to:

$$2\ ZrB_2 + 5\ O_2 \rightarrow 2\ ZrO_2 + 2\ B_2O_3$$
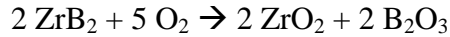
That reaction incorporates a 5 step oxidation mechanism: 1) diffusion of molecular of oxygen in the gas phase to the particle surface through the particle bed; 2) chemisorption of molecular oxygen on the surface; 3) atomic oxygen diffusion through bulk ZrB_2; 4) formation of a layer of transition phase; and 5) atomic oxygen diffusion thorough the surrounding layer to ZrB_2 powders inside.

Tripp and Grahm[38] found an increasing deviation of oxidation of ZrB_2 (hot-pressed billet from Manlabs Incorporated) from parabolic kinetics with increase in temperature at an oxygen partial pressure of 250 mm. They showed that the rate of oxygen consumption was controlled by oxygen diffusion through the B_2O_3 and that a paralinear equation could be derived for rate of oxygen consumption within their range of measurements. Kaufman and Clougherty[2] reported that ternary alloying elements substituting on the boron sub-lattice enhanced oxidation properties of these diborides. Table 2 summarizes the probable products in the oxidation experiments (under the conditions specified above) as provided by Kaufman and Clougherty[2].

Table 2. Summary of Probable Products in the Oxidation of HfB_2 and ZrB_2[2]

Compound	Temperature	Products
HfB_2	above 1488K	HfO_2 (c); B_2O_3 (g)
ZrB_2	below 1329K	ZrO_2 (c); B_2O_3 (c)
	Above 1439K	ZrO_2 (c); B_2O_3 (g)

Tripp, et al.[14] investigated the oxidation of ZrB_2+ 20% SiC and compared it with oxidation of ZrB_2. They showed that both materials oxidize similarly at temperatures < 1100^0C but differ in the range 1100^0C – 1300^0C. In that upper interval SiC oxidizes and forms appreciable amounts of glass, which improves the oxidation resistance of the material. This work indicated that the rate of oxidation reaction is controlled by inward diffusion of oxygen through the glass phase. A recent study of reactive hot pressing of ZrB_2-SiC composites by Zhang, et al.[9] showed that B and C atoms diffuse into Zr and Si sites and form ZrB_2 and SiC respectively. This diffusion is slow and the microstructure of the obtained composite possesses the features of the zirconium and silicon starting powders. The conclusion drawn from all these studies is that oxidation of ZrB_2 is controlled by oxygen diffusion and the material properties of ZrB_2 such as oxidation resistance and thermal shock resistance can be enhanced by addition of SiC.

Thermal Properties: Thermal diffusivity data are necessary for modeling transient heat conduction in materials and are essential for designing thermal protection systems. Thermal diffusivity is a measure of the time it takes a material to reach thermal equilibrium when subject to transient heating events and is defined as the ratio of thermal conductivity to the product of specific heat and density.

$$\alpha = \frac{k}{\rho \cdot C_p},$$

Here α is the thermal diffusivity, k is the thermal conductivity, ρ is the density, and C_p is the specific heat. Previous research on the thermal properties of HfB_2, ZrB_2, HfB_2-SiC, and ZrB_2-SiC are limited. The one exception to this is the results of measurements of the specific heat of HfB_2 and ZrB_2 that can all be found in the TPRC data collection.[7]

Because many UHTC materials contain several phases, their thermal properties must be analyzed using multiphase conduction models.   For example, the thermal diffusivity of a two-component composite can be estimated using 2-phase conductivity models if the properties of each individual component are known. Likewise, if the thermal diffusivity of a composite is known, the values of the pure components can be estimated from the models.   This is particularly useful in cases where it is impractical to measure the properties of the pure components. Ohm's law models are the simplest 2-phase conduction models, for example the series and parallel conduction models where the two different materials are assumed to be in layers either parallel or perpendicular to the heat flow. These models define the upper and lower bounds of conductivity in composite systems. In addition to the series and parallel models, the geometric mean model is one that approximately represents the midpoint between the upper and lower bounds. Two other models of importance are based on effective medium theory. The Maxwell[12] model predicts the effective conductivity by assuming randomly distributed, non-interacting spheres in a matrix with different properties. The Bruggeman model[12] assumes the matrix and inclusion are both symmetrically distributed. The Bruggeman model eliminates the randomness of the Maxwell model and improves its validity for higher inclusion concentrations[12]. However both models have their limitations, as is discussed in

the general review by Taylor[13]. Choy gives a thorough review of the Maxwell and Bruggeman theories and their limitations[12].

Experimental Results

Processing: One of the major accomplishments of this project was learning how to make superior UHTCs and then determining the properties needed to make intelligent design decisions. We made ZrB_2 – SiC and HfB_2 – SiC UHTCs with excellent properties in compositions as low as 2 vol% SiC. The results of the hot pressing experiments are shown in Figure 3, which is a plot of specimen density as a percentage of the theoretical value as a function of SiC content. Previous attempts by others to make thermal protection materials in these same systems required 20% SiC. The results of the present work demonstrated a wider range of compositions than was previously known, which gives designers more options in optimizing thermal protection systems (TPS).

The UHTCs studied here were made by hot-pressing powder mixtures in graphite dies. All specimens were sintered at 2000°C and 5000 psi, using a ramp rate of 20°C/min, held at 2000°C for one hour, and then cooled by turning off the power to the furnace. The hot press was a Centorr model running under an atmosphere of gettered argon gas at 5 psi. The graphite dies were lined with Grafoil brand graphite tape (Union Carbide) to protect the dies from reacting with the powders. Samples with diameters from 2.54 cm to 6.35 cm were produced. The aspect ratios, or the height-to-diameter ratios, ranged from 0.12 to 1.10.

CERAC Inc., Milwaukee, Wisconsin, supplied the powders. The manufacturer's specifications for these powders are shown in Table 3.

Table 3. Starting material composition, purity, and other specifications.

Material	Chemical Formula	Molecular Weight (g/mol)	Purity	Size	Density (g/cm^3)
Hafnium Diboride	HfB_2	200.11	0.995	325 mesh	10.5
Zirconium Diboride	ZrB_2	112.84	0.995	325 mesh	6.085
Silicon Carbide	SiC	40.09	0.990	325 mesh	3.22
Silicon Carbide	SiC	40.09	0.999	< 1 micron average	3.22

The powders were prepared by mixing the diboride powder with the desired amount of silicon carbide and then milling the mixture. Both ball milling and attritor milling were used, as was dry milling in a Spex mill with a tungsten carbide ball.

Most samples were prepared by ball milling the powders using zirconia media in hexane for 8 to 10 hours. For attritor milling, the powders were milled using silicon carbide media and hexane for approximately 1 hour at 600 rpm. Batch size was 250 cm^3. In the attritor milled samples, weight loss from the SiC media was added to the silicon carbide content of the powder to arrive approximately at 2, 5, 10, and 20 vol% SiC in the diboride.

The samples and their specifications are listed in Table 4.

Table 4. Sample specifications. This table lists the silicon carbide content, the theoretical density, and what measurements were made on each sample (C_p is the specific heat at constant pressure, CTE is the coefficient of thermal expansion, α is the thermal diffusivity). (*attritor milled, **Spex milled).

	Sample	vol% SiC	Density (g/cm^3)	Fractional Theoretical Density	SiC Purity	Where Used
	2	0	4.57	0.75	n/a	C_p, CTE
	3	0	4.52	0.74	n/a	α
	7	2	5.93	0.98	0.99	C_p
	28**	5	5.26	0.88	0.999	α, CTE
	6	5	5.88	0.99	0.99	C_p
ZrB$_2$	5	5	5.91	0.99	0.99	C_p
	33*	5	6.02	1.01	0.999	α, CTE
	32*	10	5.87	1.01	0.999	α, CTE
	27**	20	5.32	0.97	0.999	α, CTE
	29*	20	5.49	1.00	0.999	α, CTE
	4	20	5.51	1.00	0.99	C_p
	8	0	7.17	0.68	n/a	α, C_p, CTE
	12	0	7.22	0.69	n/a	α
HfB$_2$	11	2	10.48	1.01	0.99	α, C_p, CTE
	19	5	9.61	0.95	0.99	α
	10	5	10.19	1.01	0.99	α, C_p, CTE
	18	20	9.33	1.03	0.999	α, C_p, CTE

Figure 3 presents results of hot pressing experiments for HfB_2 – SiC and ZrB_2 – SiC UHTCs. One of the outstanding scientific issues in processing the UHTCs is why at least 2% of additives such as SiC or WC are required to achieve full density in hot pressing. One possibility is that the UHTCs densify by a liquid phase sintering mechanism, but until now there has been no evidence for such a mechanism. This question is of more than academic interest because, if the densification mechanism were known, it should be possible to devise a pressureless sintering process that would allow us to make bigger parts much more cheaply, and possibly with better high temperature properties.

% Theoretical Density Vs. SiC Content
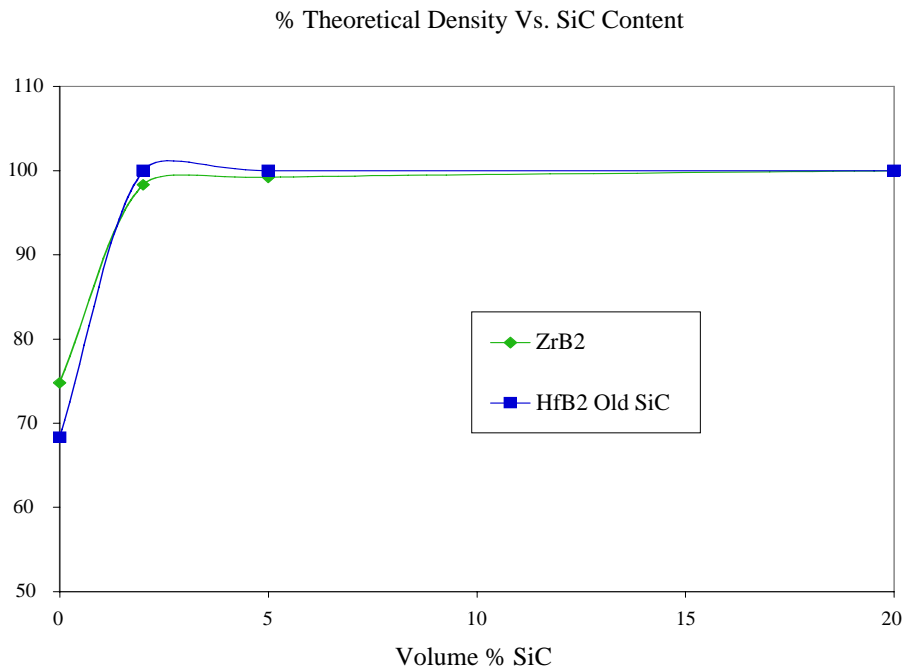
Figure 3: Variation in the relative density of ZrB_2-SiC and HfB_2-SiC ceramics as a function of SiC content. The ceramics were prepared by hot pressing at 2000°C and 5000 psi. Note that full density is obtained for all compositions with 2vol% or more SiC.

Microstructures: Polished cross sections of the hot-pressed samples were examined to characterize their microstructures. Sample images were collected and analyzed for grain sizes, and phase areas. Collected data consisted of:

1. Metal diboride average grain size

2. SiC/Pore average grain size

3. Inclusion area, percent

SEM images were used for this analysis. Most images were taken at 3000x but samples 8, 12, and 19 (Table 4 above) were taken at 1000x. Samples 29, 32, and 33 were not polished sections but were micrographs of fracture surfaces. Each image was selected to be representative of the bulk microstructure.

The image analysis was done with the National Institute of Health's ImageJ software, v. 1.30.[15] The SiC phase and the pores were indistinguishable using the image analysis software with the scanning electron microscope (SEM) images. Therefore, the reported average grain size is the average for both SiC and the porosity. This qualification applies to the inclusion area as well. The inability to distinguish pores from the SiC phase in the SEM images is the reason the SiC additions and theoretical densities were used instead of these microstructural measurements in modeling of composite thermal properties. The metal diboride average grain sizes were measured by a combination of the line intercept method and individual grain measurements.

The micrographs of the HfB_2 based samples are shown below in Figures 4 through 9. They are arranged in order of increasing SiC content. The scale for each figure is indicated in the captions.
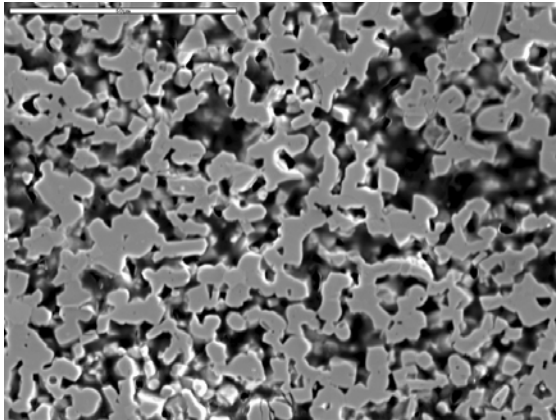
Figure 4. Sample 8, HfB_2+0% SiC (bar is 50μm).
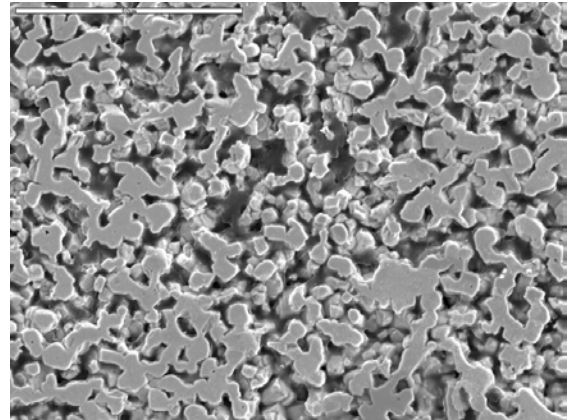
Figure 5. Sample 12, HfB_2+0% SiC (bar is 50μm).
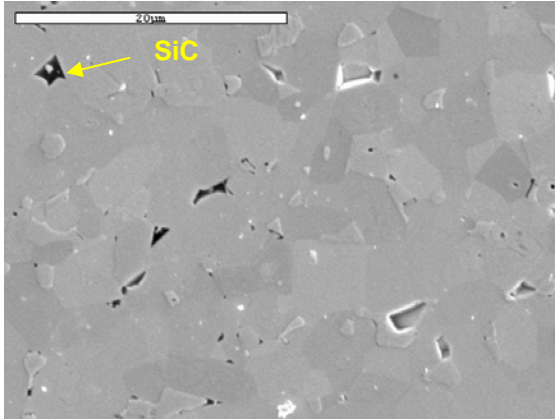
Figure 6. Sample 11, HfB$_2$+2% SiC (bar is 20μm).
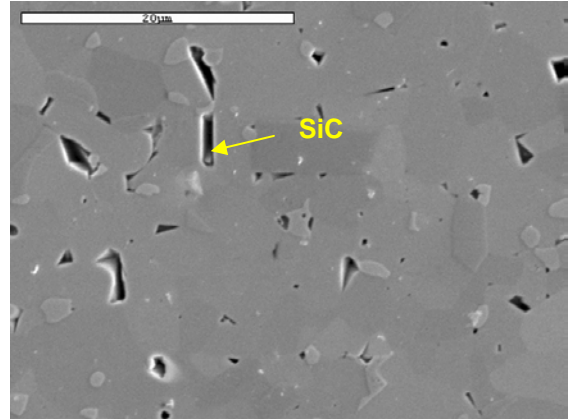
Figure 7. Sample 10, HfB$_2$+5% SiC (bar is 20μm).
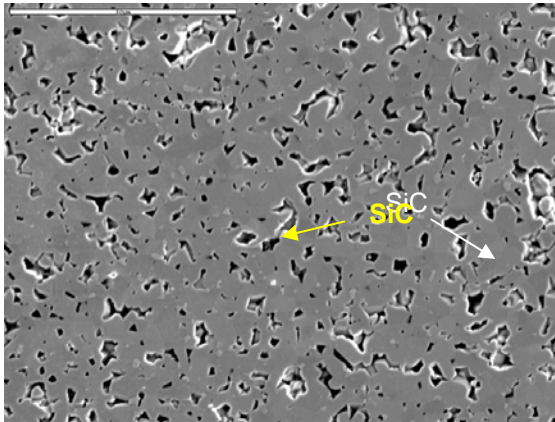
Figure 8. Sample 19, HfB$_2$+5% SiC (bar is 50μm).
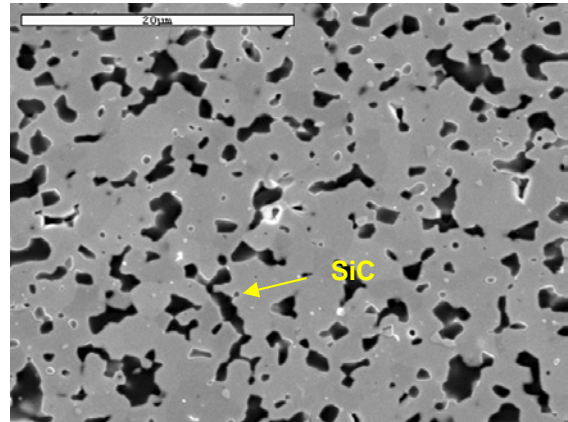
Figure 9. Sample 18, HfB$_2$+20% SiC (bar is 20μm).

The micrographs of the ZrB$_2$ based samples are shown in Figures 10 through 15. They are arranged in order of increasing SiC content. Figures 11, 13, and 15 are images of fracture surfaces instead of polished sections.
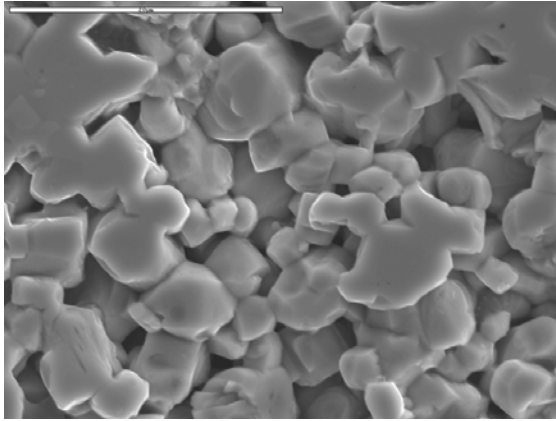
Figure 10. Sample 3, ZrB_2+0% SiC (bar is 20μm).
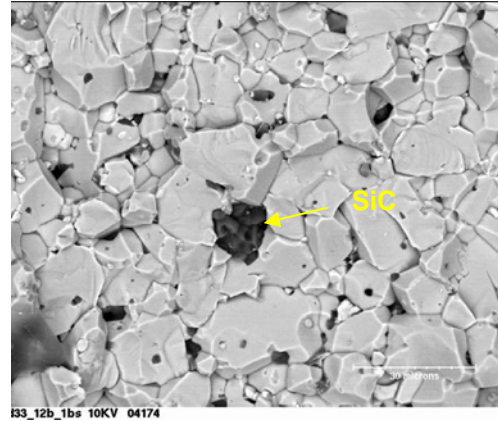
Figure 11. Sample 33, ZrB_2 + 2% SiC (bar is 30μm, fracture surface).
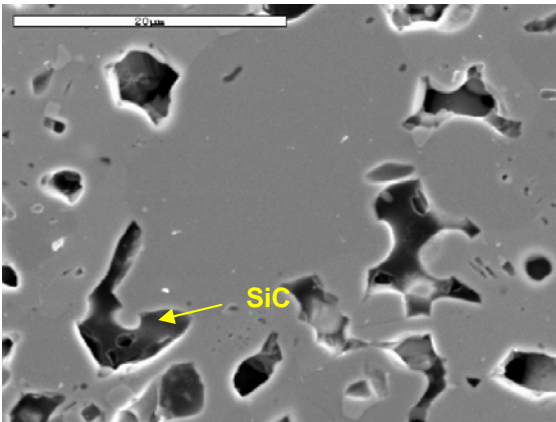
Figure 12. Sample 28, ZrB_2+5% SiC (bar is 20μm)
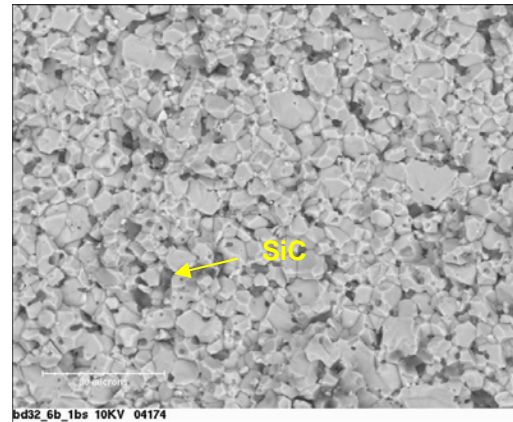
Figure 13. Sample 32, ZrB_2+10% SiC (bar is 30μm, fracture surface).
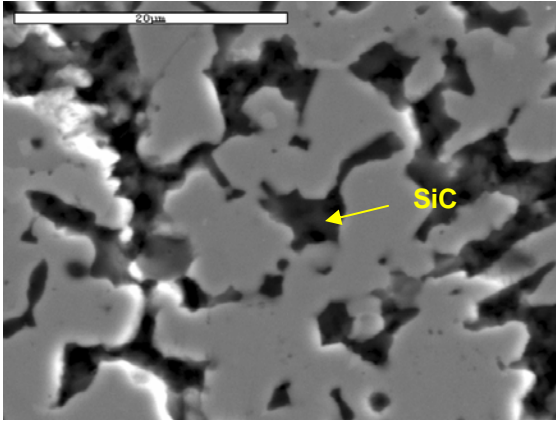
Figure 14. Sample 27, ZrB_2+20% SiC (bar is 20μm).
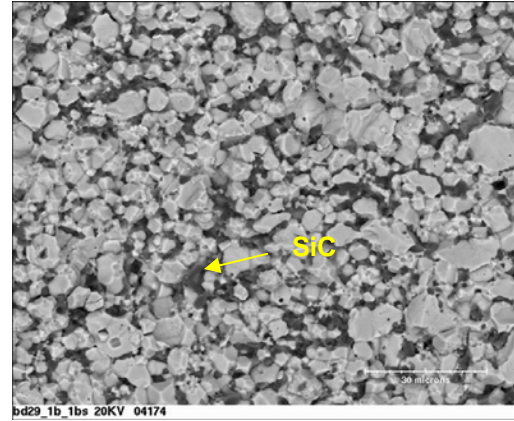
Figure 15. Sample 29, ZrB_2+20% SiC (bar is 30μm, fracture surface).

The SiC contents and porosity were measured from the above micrographs and compared to the SiC additions and the porosity (as measured by the Archimedes method) for each sample. Note that in Table 5 how the measured inclusion area is roughly the same as the sum of the SiC volume additions and the porosity.

Table 5. Average grain sizes and inclusion areas for samples used in the thermal diffusivity testing. Notice the increase in SiC/pore grain size with the 20% SiC additions, the larger SiC/pore grain size in samples 27 and 28, which is likely due to less milling time, and the abnormally large MB_2 grain size for sample 33.

| | | | Measured from Micrographs | | |
| | *SiC addition, %* | *Porosity, %* | **Inclusion Area (SiC+porosity), %** | **SiC/pore grain size, μm** | **MB_2 grain size, μm** |
Sample					
3	0	26	n/a	n/a	5
8	0	32	n/a	n/a	3
10	5	0	2	0.5	3
11	2	0	1	0.5	3
12	0	31	25	5	4
18	20	0	20	1	3
19	5	5	11	1	3
27	20	3	22	6	5
28	5	12	14	3	6
29	20	0	21	3	4
32	10	0	9	1	4
33	2	0	5	2	8

High Resolution Microstructural Analysis: If the UHTCs densify by a liquid phase sintering mechanism we would expect to find evidence of second phases on the grain boundaries in the dense ceramics. Previous attempts using scanning and transmission electron microscopy did not show any residual grain boundary phases and thus the role of the additives and how they affected the densification were unclear. Our microstructural analysis using high resolution electron microscopy, coupled with Sandia's spectral image analysis technique, provided the first evidence of grain boundary phases in the UHTCs. Very narrow silicate grain boundary phases some tens of nanometers thick were observed and their compositions and locations were determined. Although much more extensive analysis will be required to reach a definitive conclusion, the results obtained from this LDRD suggested that oxide impurities in the SiC additives react at 2000°C to make a small amount of liquid that promotes densification. Softening of such phases could explain the observed fall-off in strength at 1000 - 1200°C.
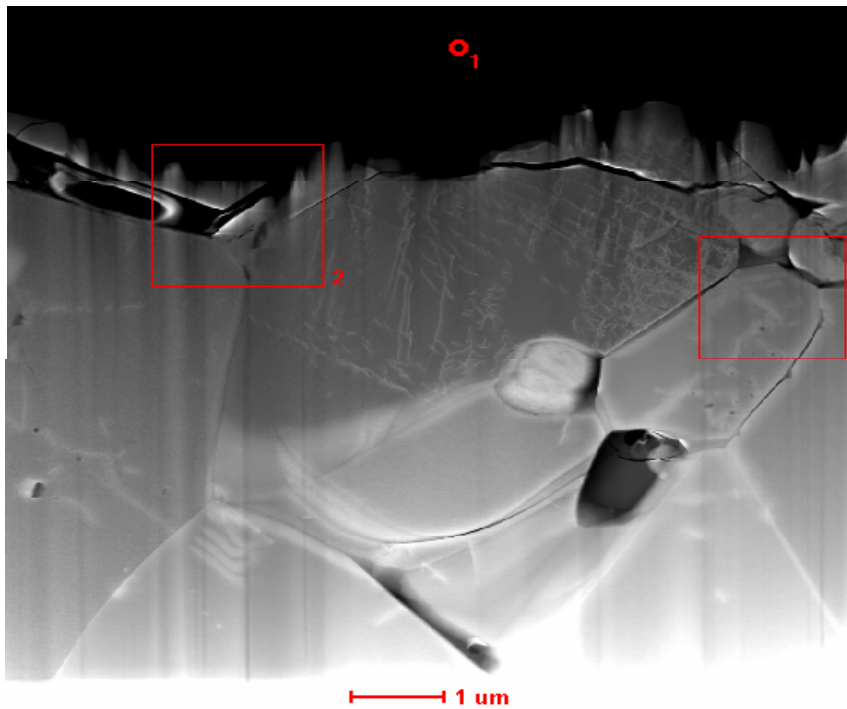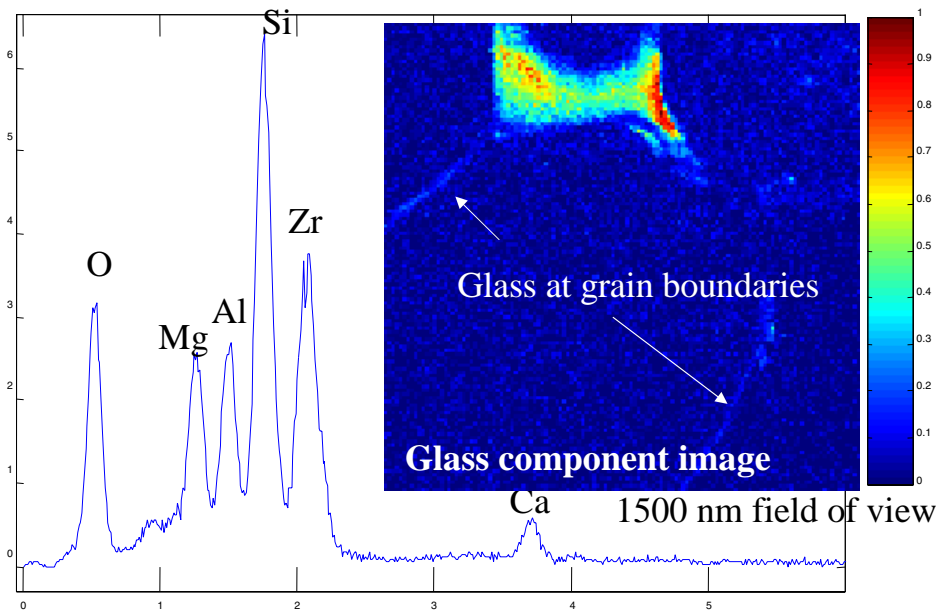
Figure 16: Upper figure is the electron micrograph of a $ZrB_2 - 2\%$ SiC ceramic. The spectral image of the right hand area outlined in red in the upper right is shown in the lower figure.

Mechanical Properties: We measured the mechanical properties of our ZrB_2- and HfB_2-based UHTCs to determine the relation between properties, microstructure, and processing. We measured the fracture toughness for ZrB_2-SiC with SiC contents of 5, 10, and 20vol% SiC using the chevron notch technique. This method is more difficult than the popular diamond indent technique, but it gives much more reliable results for multiphase ceramics such as these UHTCs. We determined room temperature fracture toughness values (K_{1c}) of 5.1 to 6.2 MPa m$^{1/2}$, with no systematic dependence on composition. These values are quite good, particularly for ceramics that have not been optimized for their mechanical properties. It is worth noting that these values are about 50% higher than the ones reported recently for $HfB_2 - 20\%$ SiC material. Figure 17 is a micrograph of the fracture surface of a chevron notched specimen after breaking it at room temperature.

Strength at high temperatures is an important property for TPS materials. We measured the strengths of $ZrB_2 - $ SiC and $HfB_2 - $ SiC specimens in four point flexure at room temperature, 900°, and 1450°C using the ASTM C 1211 procedure with test bars with an inner span of 20 mm and an outer span of 40 mm. Figure 18 shows the results of these measurements on UHTCs with a range of compositions. The specimens tested at the highest temperatures showed a drop in strength above 1000°C. This behavior has been

attributed to softening of a grain boundary phase at high temperatures. The best specimens exhibited very respectable strengths of around 450 – 500 MPa at temperatures below the high temperature strength decrease.
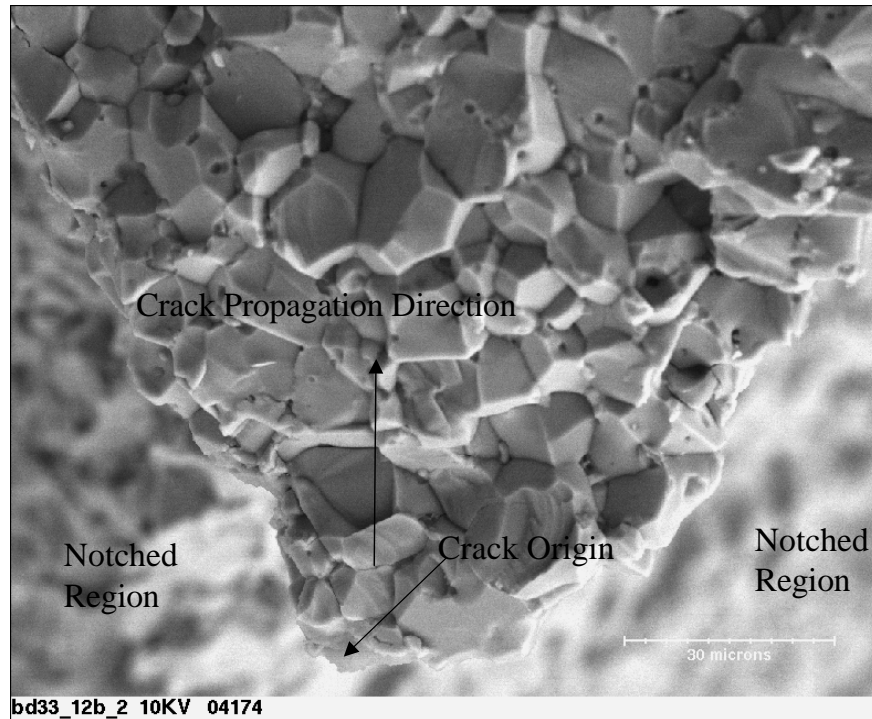
Figure 17: **Micrograph of the fracture region in a chevron notch test for ZrB_2 – 20 vol% SiC.** Fracture toughness was measured as 6.4 MPa m$^{1/2}$
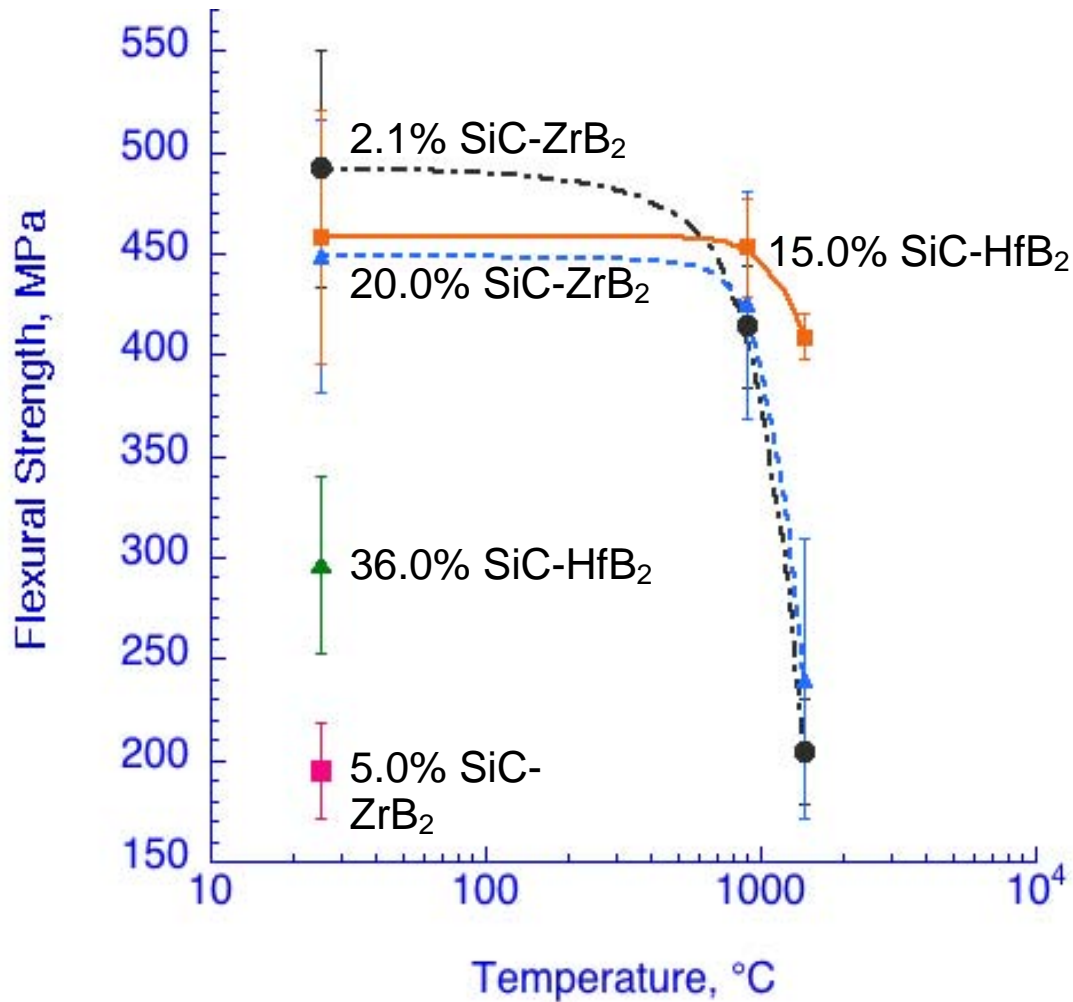
Figure 18: Variation of 4-point flexure strength as a function of temperature for UHTCs.

Thermal Diffusivity: The thermal diffusivity was measured on an Anter Flashline 5000 laser flash diffusivity instrument according to ASTM 1461-01, the "Standard Test Method for Thermal Diffusivity by the Flash Method"[18]. The Anter Flashline 5000 was equipped with a graphite furnace capable of 2000°C. The temperature was measured by two optical pyrometers, one for the low and one for the high temperatures. The flash source was a Nd:YAG laser utilizing fiber optic delivery for a uniform beam and to provide distance between the laser power supply and the measuring instrumentation. The signal from the laser was measured by an InSb detector below 900°C and by a silicon photodiode above 900°C. There was noise present in all signals, which were smoothed by applying a frequency cutoff of 50 Hz and a bandwidth of 20 Hz. The accuracy of this smoothing method, the automatic calculation of the diffusivity, and the accuracy of the pyrometers were all verified by running a graphite standard and comparing the results to NBS reported values[19].

25

The flash diffusivity method typically does not require calibration, as it is a direct measurement of a thermal property[18], but a calibration was done anyway to verify the data acquisition and analysis. A NIST graphite standard (Poco Graphite AXM-5Q1) was selected because it could withstand both the range of temperatures required and because its thermal diffusivity was similar to that of pure zirconium diboride and hafnium diboride. For example, at 1000°C the diffusivities were approximately 0.14, 0.20, and 0.17 for AXM-5Q1 graphite, ZrB_2, and HfB_2 respectively (from experimental measurements and NBS values). Values for the graphite are from NBS Special Publication 260-89[19]. The results of the calibration are shown in Figure 19.
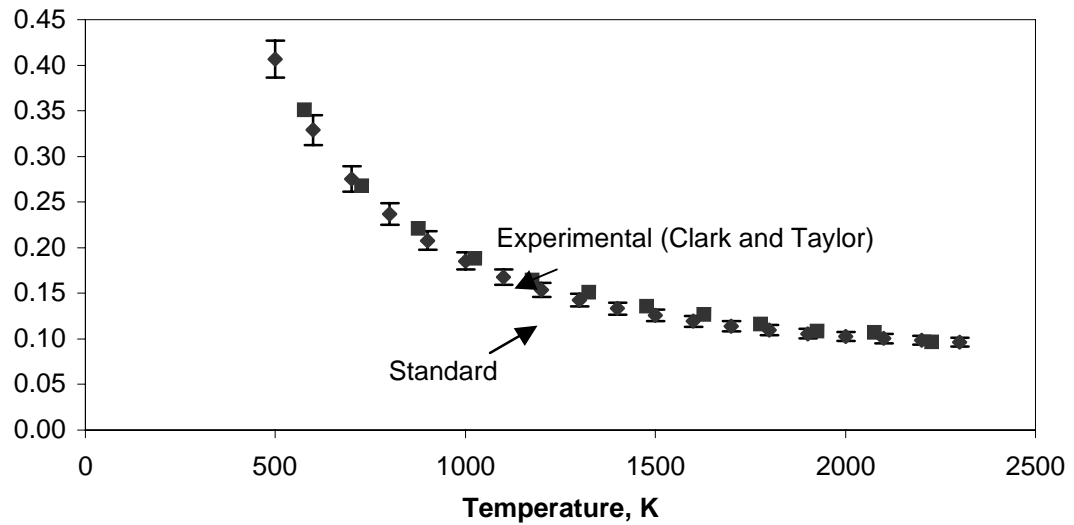
Figure 19. Experimentally measured values of an AXM-5Q1 graphite standard. The error bars represent a 5% error.

The software supplied with the apparatus uses 5 different analysis methods to compute the thermal diffusivity. These methods are the Parker[20], Heckman[21], Cowan[22], Clark and Taylor[23], and Degiovanni[24] methods. Each analysis method, except for the Parker method, uses a different approach to correct for deviations from the ideal caused by factors such as radiative cooling, 2-D heat flow, and others. The calibration was used to determine which analysis provided the best fit for these UHTCs over the temperature range of interest. The calibration revealed that the Clark and Taylor method was the most accurate of these five methods over all temperatures and therefore was used for all the experiments reported here. For a more thorough description of these methods, see the excellent review by Thermitus[24]. The samples were cut from 25.4 mm diameter pellets

26

that ranged from 3 to 5 mm thick, which resulted in a peak signal between 60 and 160 ms after the laser pulse. The surfaces were ground using a 10 mm wide diamond grinder to remove carbides and the graphite left over from the hot pressing. The efficiency of the grinding procedure was checked by x-ray diffraction, which revealed no carbides or other impurities, to the resolution of the instrument. The surface grinding was done in short steps of 25.4 μm or less to prevent the formation of cracks and followed the general machining guidelines described in ASTM 1470-00, "Testing the Thermal Properties of Advanced Ceramics"[23]. A diamond saw was used to cut the sample to shape.

The flash diffusivity method is particularly sensitive to sample surface finish and thickness variations and requires precise machining[25]. The surfaces were made uniformly smooth by polishing the faces with 600 grit SiC paper. To ensure the samples all had the same laser absorptivity and emissivity, all samples were coated with a very thin layer of graphite from an aerosol spray can. The thicknesses were measured using a micrometer.

Each sample was tested a minimum of 6 times at each temperature of 250, 500, 750, 1000, 1250, 1500, 1750, and 2000°C. The samples were held in a graphite holder in an atmosphere of ultra high purity argon at 5 psi and with a flow rate that was approximately 2 liters per minute.

Data Analysis

Thermal properties data analysis: The thermal diffusivity is defined as $\alpha = \kappa/(\rho\, C_p)$, where κ is the thermal conductivity, ρ is the density, and C_p is the specific heat at constant pressure. The temperature dependence of each term is as follows: The thermal conductivity has a temperature dependence[26] of $1/T$, the density has a direct temperature dependence T, and the specific heat can be fit to a temperature dependence of $A + BT^{-1} + CT^{-2}$. Because the dependency of density on temperature is much smaller than the dependence of κ and C_p, the resulting overall temperature dependency is $1/T$.

Thermal conductivity is a measure of the steady state heat transfer rate. It can be combined with the density and the specific heat to determine the thermal diffusivity. Alternatively, the thermal conductivity can be calculated from the thermal diffusivity and specific heat, as was done in this work, and as is usually the case in such research. The present calculations used both measured and extrapolated specific heat data. The extrapolations to higher temperature were based on a logarithmic curve fit to the measured values. The reasonableness of this extrapolation was ascertained by comparing the curve fit to published TPRC data[7]. Based on the ASTM standards for each measurement, thermal diffusivity is estimated to be accurate within 5%, density to better than 1%, and specific heat to 8.4%. Adding the errors together results in an estimated 15% error for the calculation.

Specific Heat: Specific heat was necessary for calculating the thermal conductivity based on the relation, $k = \alpha\rho C_p$, where k is thermal conductivity, α is thermal diffusivity, ρ density, and C_p is specific heat at constant pressure. With information on the diffusivity, the density of the material, and the heat capacity, the thermal conductivity can

be determined. The specific heat was measured using a TA Instruments DSC-2010 differential scanning calorimeter (DSC) according to ASTM E 1269-99[27]. A sapphire standard was used to perform the heat flow calibrations each day a test was run.

At least one sample of each of the eight unique compositions was selected for specific heat measurements (see Table 4 for the specific samples used). The samples were prepared by cutting the hot-pressed compacts to produce thin, flat specimens resembling the sapphire standard. The mass of each sample was between 17 and 50 mg. After cutting, the samples were conditioned either in a separate box furnace or within the DSC unit itself. In both cases, conditioning consisted of heating the samples up to the maximum temperature expected in the DSC and holding there for a minimum of 2 minutes. This follows the recommended practice for conditioning the sapphire sample as reported in ASTM E 968-99 10.2.2[28].

The samples were placed inside aluminum pans and covered with aluminum lids. The pan and lid combination typically weighed around 25 mg. The same pan and lid combination, or a weight-matched pan and lid (within 0.1%) were used throughout each experiment.

Samples were tested from 100°C to 350°C. The tests were not run above 350°C because of difficulties in getting repeatable data, possibly due to an interaction with the aluminum pans (some discoloration was observed above this temperature). The ramp segment started 50°C before and ended 25°C after the desired specific heat range and the samples were equilibrated for 10 minutes at these starting and ending temperatures. An inert cover gas of ultra high purity argon was used at 44 ml/min and 5 psi. After the experiments, all samples were weighed to check for mass loss. Runs on each sample were repeated until three consistent specific heat measurements were obtained. The first run was typically a conditioning run. Reported measurements are an average of the three or more consistent repeat values obtained for each sample.

Calculation of the specific heat was performed by TA Instrument's Specialty Library V. 1.4 program (Build 1.4.0.18).

Extrapolated specific heat data were required because our DSC was limited to 600°C. These data were further restricted to 350°C because of a lack of reproducibility above this temperature. A logarithmic curve fit was applied to the data from the pure ZrB_2 and HfB_2 samples using Microsoft Excel. The curve fit was assumed reasonable after comparison with the TPRC[7] and NIST data[29] (see Figure 20).
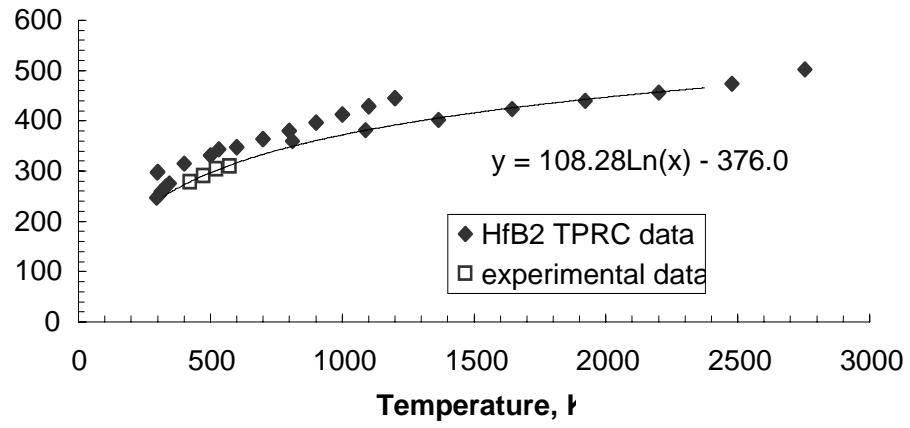
Figure 20a. Specific heat data used for calculating the thermal conductivity of HfB$_2$.

(b)

Specific heat, J/kg/K (y-axis) vs Temperature, K (x-axis)

$y = 343.84 \text{Ln}(x) - 1225.59$

♦ SiC NIST data
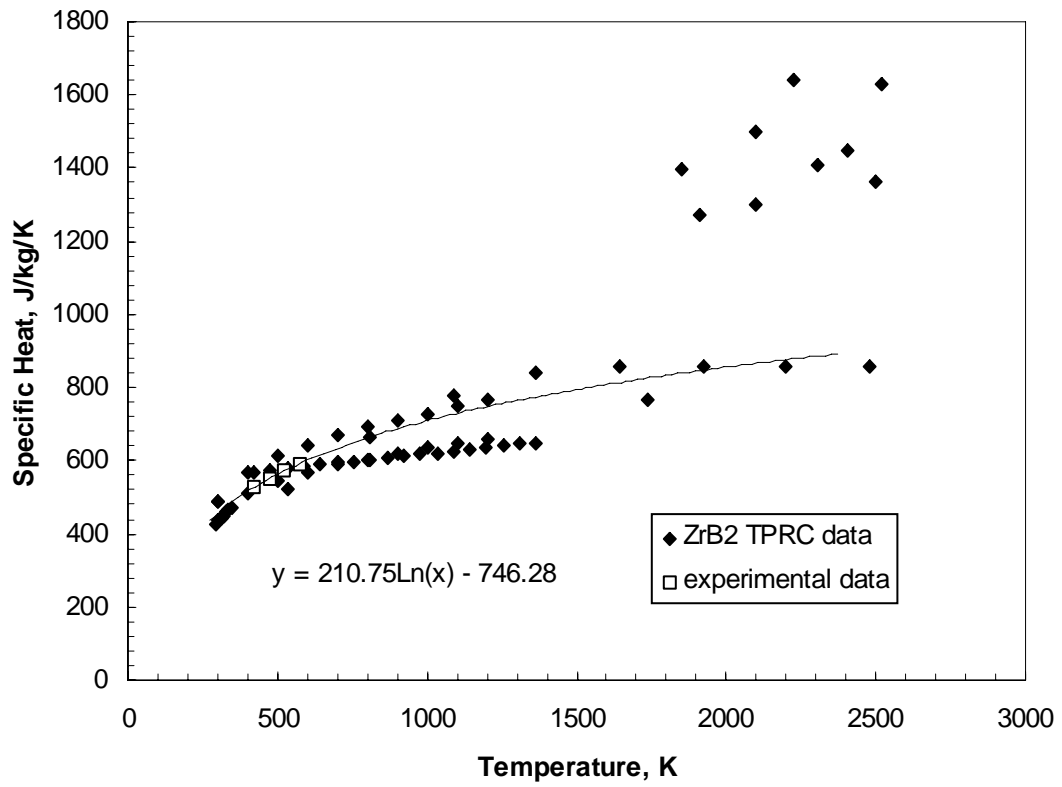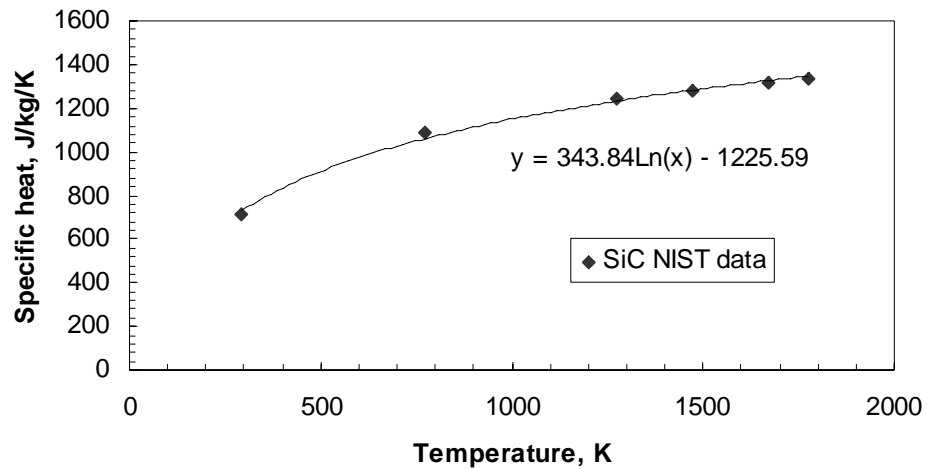
(c)

Figures 20b and 20c: Specific heat data used for calculating the thermal conductivity for ZrB_2 and SiC.

The curve fit data were then combined using the rule of mixtures to obtain the combined specific heat for each composite. To use the rule of mixtures, the volume percents were first converted into weight percents.

As shown in Table 6, there was an unexpected trend of decreasing specific heat with SiC content, except for the samples with 20 vol% SiC. This is a counterintuitive trend because the specific heat of SiC is larger than all the values shown here. By the rule-of-mixtures the specific heat should increase with SiC content. Large variability in data was also seen between some runs, which could explain the observed results.

Table 6. Specific heats of various UHTC compositions.

Material System	Sample #	SiC, %	Specific Heat, J/(kg*K)			
			150°C	200°C	250°C	300°C
HfB$_2$+SiC	8	0	278	291	304	310
	11	2	272	285	298	305
	10	5	255	265	271	265
	18	20	280	295	304	309
ZrB$_2$+SiC	2	0	528	552	573	592
	7	2	525	549	567	584
	5 and 6	5	493	516	532	544
	4	20	563	599	625	645

Thermal Expansion: Thermal expansions were measured for use in calculating the density change with temperature and to provide further thermomechanical properties of these UHTC ceramics for use in design of TPS structures. The thermal expansion was measured on a Netzsch dual-rod dilatometer, Model DIL 402ED, and analyzed using Netzsch Thermal Analysis software Version 3.6. The tests were conducted in stagnant helium at 2 psi and a heating rate of 10°C/min. The reference materials were various lengths of Netzsch alumina standards.

The UHTC expansion samples were all cut directly from the hot pressed billets and were generally ground to dimensions within 1% of the standards used for comparison. The exceptions to the 1% tolerance were samples in the 12 mm range, which were all measured with the same 12.598 mm alumina standard. The ends of the UHTC specimens were ground flat using 600 grit SiC paper with a steel block to maintain parallelism. The samples were not conditioned before testing and had no prior thermal exposure after hot pressing. The test sample number, composition, and initial length are shown below in Table 7.

Table 7. Sample number, composition, and initial length of materials used in the thermal expansion measurements.

Sample Number	Composition	Theoretical Density	Initial Length, mm
8	HfB_2+0%SiC	0.68	12.362
11	HfB_2+2%SiC	1.01	12.564
10	HfB_2+5%SiC	1.01	12.626
18	HfB_2+20%SiC	1.03	12.311
2	ZrB_2+0%SiC	0.75	8.745
33	ZrB_2+2%SiC	1.01	25.074
28	ZrB_2+5%SiC	0.88	12.047
32	ZrB_2+10%SiC	1.01	19.208
29	ZrB_2+20%SiC	1.00	19.137

As listed in Table 8, the coefficient of thermal expansion results behaved as expected. Except with the pure diborides, the coefficients of thermal expansion decreased with increasing SiC content. Data were not obtained for all materials above 1000°C because of an apparent interaction between the samples and the platinum thermocouples that caused the thermocouples to melt above 1000°C. This could have been due to the formation of PtSi within the thermocouple from the oxidation products of SiC (possibly SiO). Increased SiC content decreases the CTE as expected by the rule of mixtures.

There are some exceptions, mainly with the pure samples that do not contain SiC. The pure samples do not appear to fit the trend and we believe this may be due to microcracking in the highly porous structures in these samples. Other instances where the trend does not appear to match expectations may have been caused by measurement error associated with small sample sizes, some of which were only about between 12 to 13 mm long.

Table 8. The Coefficient of Thermal Expansion (CTE) from Room Temperature

	SiC additions	Thermal expansion coefficient (x 10^{-6})/°C					
		RT to 250°C	to 500°C	to 750°C	to 1000°C	to 1250°C	to 1500°C
ZrB_2	0% SiC	6.68	6.89	7.03	7.17	7.38	7.55
	2% SiC	6.61	6.83	7.05	7.31	7.51	7.67
	5% SiC	6.74	6.83	7.03	7.29	-	-
	10% SiC	6.45	6.67	6.88	7.08	7.26	7.53
	20% SiC	6.21	6.45	6.64	6.84	7.04	7.18
HfB_2	0% SiC	6.48	6.69	6.89	7.15	7.37	7.49
	2% SiC	6.60	6.85	7.08	7.34	7.56	7.68
	5% SiC	6.61	6.79	6.99	7.22	-	-
	20% SiC	6.10	6.23	6.45	6.73	-	-

Thermal Diffusivity: The thermal diffusivities for the HfB_2+SiC composites are shown below. Porosity has the greatest influence on the thermal diffusivity as seen in the 64% dense and 65% dense samples. In all cases the thermal diffusivity decreases with an increase in temperature. This decrease in thermal diffusivity is more pronounced in the

sample containing 20 vol% SiC. This is expected due to the low thermal diffusivity of the SiC at high temperatures.
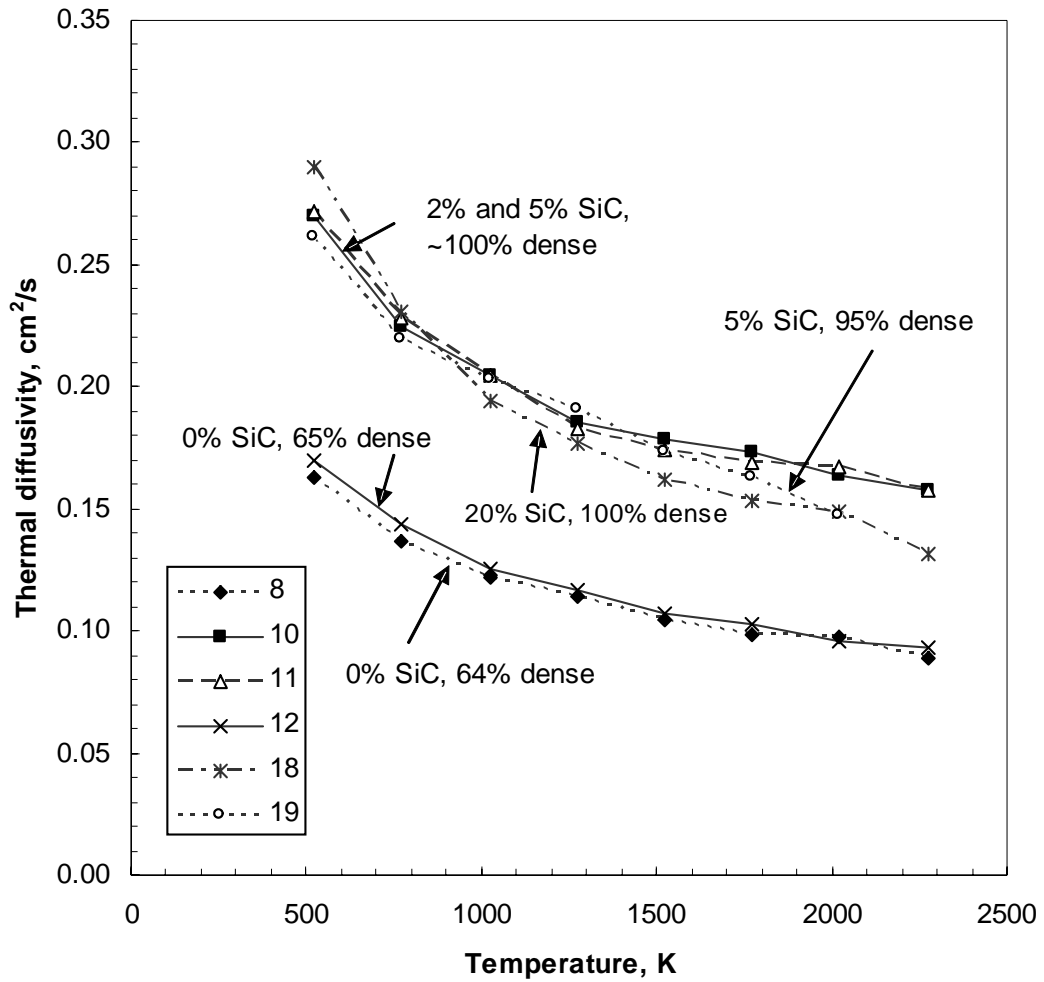
Figure 21. Thermal diffusivities of the HfB$_2$+SiC composites. Note the monotonically decreasing trend, the large drop in diffusivity with porosity, and the relatively minor effect of SiC content (except at 20 vol%), and the increased slope in the 20 vol% samples.

The ZrB$_2$-SiC composites show the same trends as seen in the HfB$_2$-SiC samples. This includes the much lower thermal diffusivity with increased porosity and the increase in
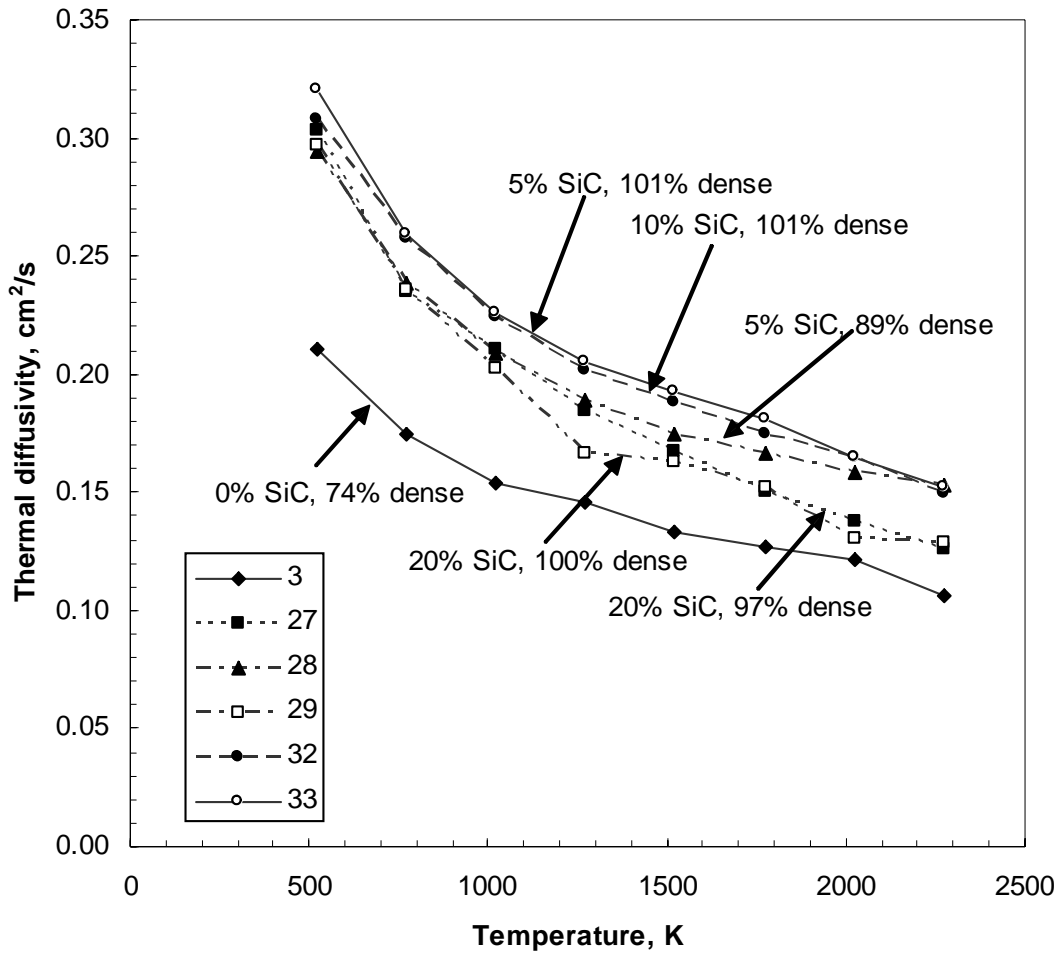
Figure 22. Thermal diffusivities of the ZrB$_2$+SiC composites. Notice the monotonically decreasing trend, the large change in thermal diffusivity with porosity, the large drop in the thermal diffusivity in the 20 vol% samples even at full density, the same increased slope with 20 vol% SiC as seen in the HfB$_2$+20%SiC sample, and the disparities between the two 20 vol% samples.

slope observed in the samples with larger SiC additions. The thermal diffusivity data are tabulated below for the HfB$_2$ based ceramics. Error estimates, calculated using the 95% confidence interval on the t-distribution, are presented next to each data point in ±%.

Table 9. Summary of the HfB$_2$ thermal diffusivity measurements with error estimates. The error estimates are based on the 95% confidence interval using the t-distribution.

Sample	8		10		11	
SiC Content	0.00		0.05		0.02	
Density (g/cm^3)	7.17		10.19		10.48	
Theoretical Density	68%		100%		101%	
SiC Grain Size	3 μm (HfB$_2$)		0.5 μm		0.5 μm	
Temperature (°C)	Thermal diffusivity (cm^2/s):					
250	0.163	1.2%	0.270	1.1%	0.272	1.1%
500	0.137	1.8%	0.225	1.7%	0.228	2.0%
750	0.122	2.0%	0.205	1.3%	0.204	1.6%
1000	0.114	5.5%	0.185	2.7%	0.183	2.6%
1250	0.105	0.9%	0.178	1.0%	0.174	1.6%
1500	0.099	2.4%	0.174	11.2%	0.169	4.3%
1750	0.098	3.2%	0.164	7.8%	0.167	5.3%
2000	0.089	10.8%	0.157	8.5%	0.158	22.2%
Sample	12		18		19	
SiC Content	0.00		0.20		0.05	
Density (g/cm^3)	7.22		9.33		9.61	
Theoretical Density	69%		103%		95%	
SiC Grain Size	5 μm (HfB$_2$)		1 μm		1 μm	
Temperature (°C)	Thermal diffusivity (cm^2/s):					
250	0.170	1.1%	0.290	1.4%	0.262	1.1%
500	0.144	2.7%	0.231	2.0%	0.220	4.3%
750	0.126	4.2%	0.194	3.8%	0.203	1.7%
1000	0.117	8.6%	0.177	5.0%	0.191	3.2%
1250	0.107	1.8%	0.162	2.7%	0.173	2.1%
1500	0.103	5.3%	0.153	1.8%	0.163	3.9%
1750	0.096	7.9%	0.149	7.9%	0.147	9.5%
2000	0.093	18.4%	0.131	9.7%	N/A	N/A

The thermal diffusivity data are tabulated in Table 10 below for the ZrB_2 based ceramics. Error estimates, calculated using the 95% confidence interval on the t-distribution, are presented next to each data point in ±%.

Table 10. Summary of the ZrB_2 thermal diffusivity measurements with error estimates. The error estimates are based on the 95% confidence interval using the t-distribution.

Sample	3		27		28	
SiC Content	0.00		0.20		0.05	
Density (g/cm^3)	4.52		5.32		5.26	
Theoretical Density (%)	74%		97%		89%	
SiC Grain Size	5 μm (ZrB_2)		6 μm		3 μm	
Temperature (°C)	Thermal diffusivity (cm^2/s):					
250	0.211	3.3%	0.303	1.1%	0.294	1.3%
500	0.174	2.5%	0.235	3.5%	0.239	3.3%
750	0.154	2.3%	0.211	3.9%	0.209	1.9%
1000	0.145	5.4%	0.185	2.7%	0.189	6.5%
1250	0.133	2.1%	0.167	0.9%	0.175	1.1%
1500	0.127	2.3%	0.150	0.9%	0.167	2.9%
1750	0.122	N/A	0.138	6.9%	0.159	5.1%
2000	0.106	5.4%	0.126	6.4%	0.153	9.1%
Sample	29		32		33	
SiC Content	0.20		0.10		0.05	
Density (g/cm^3)	5.49		5.87		6.02	
Theoretical Density (%)	100%		101%		101%	
SiC Grain Size	3 μm		1 μm		2 μm	
Temperature (°C)	Thermal diffusivity (cm^2/s):					
250	0.297	1.4%	0.308	1.7%	0.320	0.7%
500	0.235	0.6%	0.257	1.8%	0.259	1.6%
750	0.203	2.1%	0.224	2.9%	0.226	1.0%
1000	0.167	5.1%	0.201	3.7%	0.205	2.3%
1250	0.163	1.1%	0.188	1.1%	0.193	1.1%
1500	0.152	2.1%	0.175	2.1%	0.181	1.5%
1750	0.131	4.7%	0.165	3.3%	0.165	13.6%
2000	0.129	7.9%	0.150	5.4%	0.152	9.20%

Thermal Conductivity: The calculated thermal conductivities from 250 to 2000°C for the HfB$_2$+SiC and ZrB$_2$+SiC ceramics are shown below in Figures 21 and 22. These thermal conductivity values are similar to those found in metals. The ZrB$_2$-based ceramics are slightly more conductive than the HfB$_2$-based ceramics.

Figure 23. Thermal conductivities of the HfB$_2$+SiC UHTCs. These values are calculated from extrapolated specific heat data and incorporate the uncertainties associated with that extrapolation. The same trends found in the thermal diffusivity are found here in which increasing either temperature, porosity, or silicon carbide content decreases the thermal conductivity.
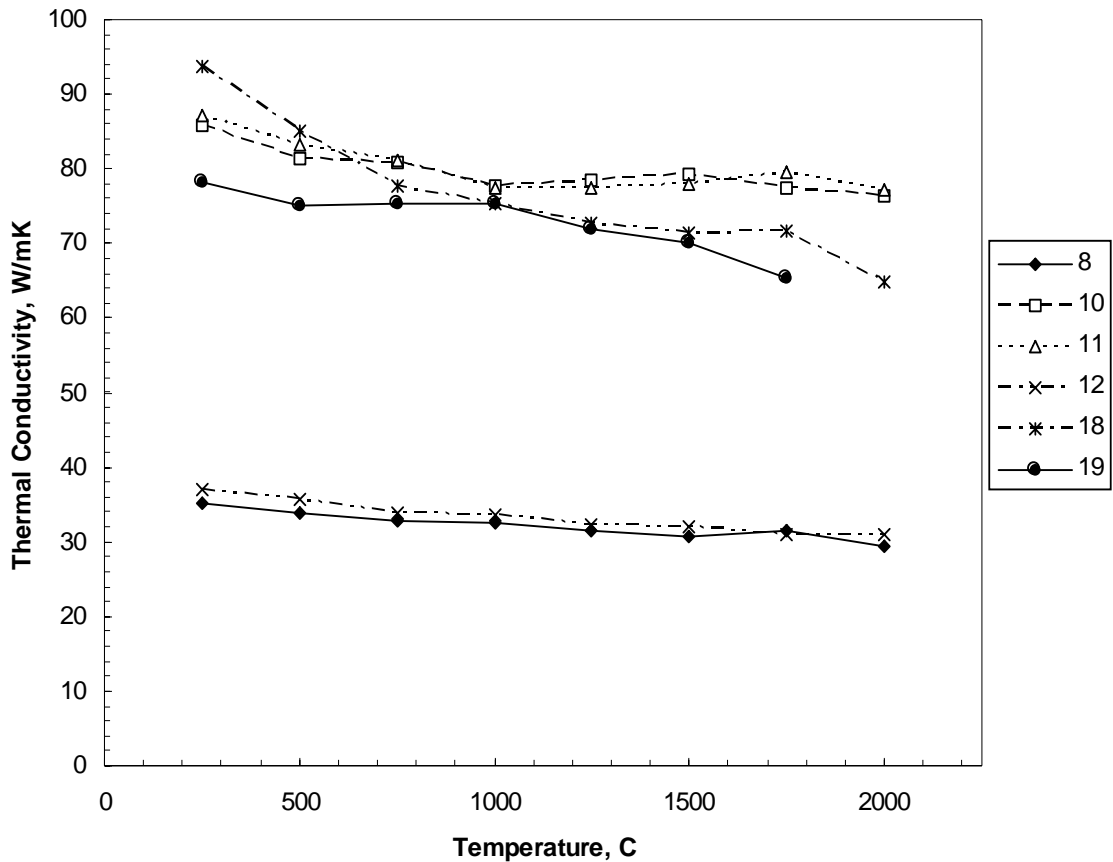
Figure 24. Thermal conductivity of the ZrB$_2$+SiC UHTCs. These values are calculated from extrapolated specific heat data and incorporate the uncertainties associated with that extrapolation. The same trends found in the thermal diffusivity are found here in which increasing either temperature, porosity, or silicon carbide content decreases the thermal conductivity.
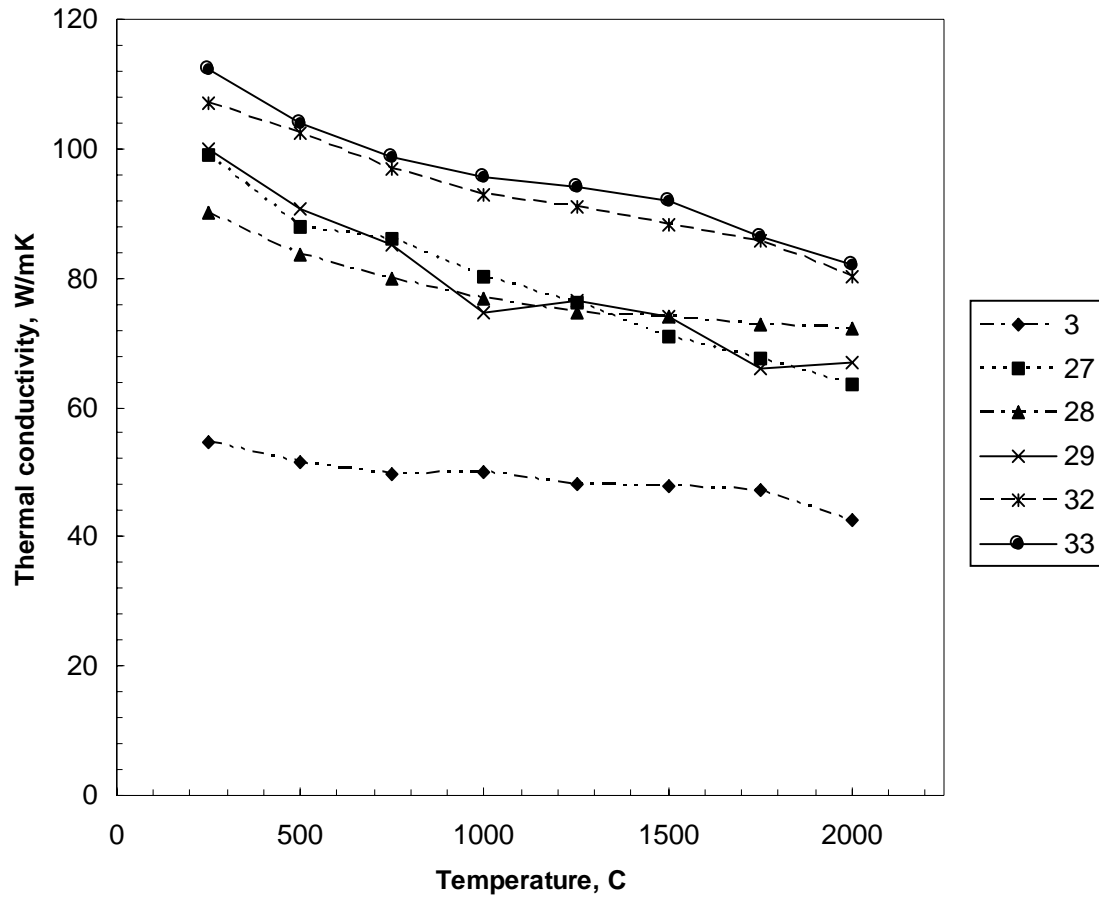
Discussion

Microstructures: Measurements of the grain sizes gave information on grain growth, agglomeration, and the effect of silicon carbide on microstructures. After hot pressing, the HfB_2 grains had an average diameter of 3.2 μm, whereas the ZrB_2 grains had an average diameter of 5.3 μm. This can be seen in Table 6, where samples 3, and 27-33 are ZrB_2 - SiC and 8-19 are HfB_2 - SiC. Initial sample preparation used ball milling of the starting powders. Later samples used attritor-milled powders. Attritor milling is a generally more powerful milling method than ball milling and produces smaller particle sizes for a given milling time. Use of attritor milling should negate the effect of different initial particle sizes in the diboride powders.

Evidence of agglomeration of SiC is present in sample 27. Agglomerates are typically detrimental to ceramic strength because of these stress concentrations. The SiC appeared to act as a grain growth inhibitor in the ZrB_2 samples. The ZrB_2 grains were significantly larger (greater than one standard deviation from the mean) in the 2% SiC than they were in either the 5%, 10% or 20% SiC samples. The HfB_2 grain size appeared unaffected by the presence of SiC. The HfB_2 grains were all tightly clustered around the mean grain size of 3.2 μm.

The results of the spectral image analysis of the diboride UHTCs show small regions at the grain boundaries with compositions that are probably derived from impurities present in the starting powders. Some regions show presence of a Si-Mg-Ca-Zr-Al-O phase that is probably glassy. These regions are very thin and were not apparent in conventional scanning electron microscopic analysis. The lack of spectral image analytical capability may be the reason that other researchers have failed to observe these thin grain boundary impurity regions. None of those elements observed in this study would have been present in pure starting powders and only the Zr, Ca and O might have been introduced from processing (from wear of the Ca-stabilized ZrO_2 milling balls). The solubility of impurity elements in the diborides is probably very low, so they would be rejected to the intergranular regions during the 2000°C hold in the hot press. The fall off in strength above 1000°C depicted in Figure 20 could be due to softening of intergranular impurity phases. If true, one approach to achieving better high temperature properties would be to devise synthetic routes to higher purity starting powders.

Processing: Because all subsequent tasks depend on availability of high quality UHTC materials, we devoted most of our initial effort to developing the process for making them. The plan was to try hot pressing initially and to attempt reactive hot pressing only if hot pressing did not produce good UHTCs. In fact, hot pressing was extremely successful and reactive processing was unnecessary. The tables below list the some of the compositions and their densities as examples of what has been produced. The theoretical densities are calculated as linear combinations of the handbook values for SiC and the diboride.

Ceramic	SiC content (vol%)	Density (g/cm³)	% of Theoretical
ZrB$_2$	0	4.57	74.8
ZrB$_2$	2	5.93	98.3
ZrB$_2$	5	5.90	98.9
ZrB$_2$	20	5.51	100

As can be seen, this LDRD project succeeded in making fully dense HfB$_2$ and ZrB$_2$ UHTCs with SiC contents down to 2%. Before this work no one had ever reported nearly full density UHTCs with less than 20% SiC and conventional wisdom was that the larger amount of SiC was necessary to achieve full density in hot pressed HfB$_2$ and ZrB$_2$. These results provide a much broader range of possible compositions for application as thermal insulation and, as discussed above, properties such as strength, thermal conductivity, and oxidation resistance vary with SiC content.

Ceramic	SiC content (vol%)	Density (g/cm³)	% of theoretical
HfB$_2$	0	7.19	68.5
HfB$_2$	2	10.48	101
HfB$_2$	5	9.90	97.4
HfB$_2$	20	9.36	103

Mechanical properties: The hot pressed specimens with 2% or more of SiC typically were at least 95% of theoretical density and were generally free of internal defects. With experience we were able to achieve room temperature strengths of 400 – 500 MPa and fracture toughness values of 5 – 6 MPam^{½}. Weaker material either had large internal process flaws such as pore or agglomerates, or the test bars had machining flaws. Properties improved with practice, for example changing from ball milling to attritor milling and substituting SiC milling balls for zirconia.

Thermal Diffusivity: The thermal diffusivities of the UHTC composites were measured from 250°C to 2000°C in increments of 250°C. The thermal diffusivities were affected by the porosity, the temperature, and the SiC content. The estimated error was also found to vary with temperature. At the higher temperatures some surface oxidation occurred that might have affected the measurements.

Porosity had the greatest effect on the thermal diffusivities. A visual comparison of the HfB$_2$-SiC data and the ZrB$_2$-SiC data (Figures 21 and 22) shows the dramatically reduced diffusivities of the porous samples, whereas all the nearly fully dense samples lie close together.

The thermal diffusivities of the UHTCs all decreased with increasing temperature, as expected. In all samples the thermal diffusivity exhibited a monotonically decreasing trend, which was the behavior expected in this temperature range. The limited number of data points were fit well by an equation of the form $A + BT + CT^{-1}$. Though the thermal diffusivity of silicon carbide is known to have a power law dependence with temperature[29], this is not known for the diborides.

Silicon carbide exhibited its greatest influence on the thermal diffusivities by reducing the porosity. By itself, it had much less of an impact. The thermal diffusivity of SiC is higher than either of the diborides at room temperature, but decreases faster, and is much lower at 2000°C. This difference in slope can be seen to affect the 20 vol% SiC samples, 18, 27, and 29, in Figures 21 and 22. The thermal diffusivities of these samples decrease faster than the others.

As shown in Tables 9 and 10 the error in each measurement was a function of temperature. There was typically a large jump in error at 1000°C and again at 1750°C and 2000°C. This error was determined by finding the 95% confidence interval using the t-distribution, which takes into account the small number of samples used for each measurement. The jump in error at 1000°C was likely due to a change in detectors required by the apparatus. At approximately 900°C, the apparatus switches from an indium antimonide detector to a silicon photodetector. At 1000°C the silicon photodetector was at its lower range of detection and therefore it was noisier. This larger noise was also evident at 1750°C and 2000°C. It was believed that this noise was the cause of the increased error at 1000°C and at the higher temperatures. Overall, the uncertainties are typical for measurements of this type. ASTM E 1461-01 states that the measurement is typically accurate to within 5%[18].

In addition to detector noise there was some oxidation of the samples at the highest temperatures. This oxidation was very slight and was observed as a graying of the material surface. Oxidation will primarily alter the surface properties to affect the absorption of heat from the laser and its reradiation. These oxidation layers were thin and could be removed easily with 600 grit SiC paper. The oxidation is not judged as significant because of the thinness of the layer, the insignificance of the total heat absorbed, and the short time of testing.

Oxidation could affect the total heat absorbed but the total heat is not crucial to the thermal diffusivity calculation. Of greater importance to measurement accuracy is the rapid absorption of heat in the top layer of the sample, which was why the graphite coating was applied. As heat deposition deviates from a step function it could create finite pulse time errors, evident as a delayed onset of the heat rise curve[18]. This delayed onset was not observed when the sample curves were normalized to the half time and the peak temperature signal and compared to the Parker model[20].

Heat loss from radiation occurred in every sample, but the possibility of increased radiation due to oxidation was not evaluated in detail. The Clark and Taylor method of analysis[23], used to calculate the thermal diffusivities in this research, modifies the measured diffusivity based on radiation losses during the rising part of the heat signal. This analysis should also compensate for any change in radiation losses due to oxidation. This oxidation was considered negligible below 1500°C due to the natural oxidation resistance of this material, and the lack of a gray layer on samples removed from the apparatus after reaching 1250°C.

A change in radiative processes caused by slight oxidation was also considered minimal because of the speed of measurement. In these experiments, the time for the signal to reach half its maximum temperature (the half time), were in the 30 to 80 millisecond range. This short time reduces the total radiation losses to a minimum compared to other thermal diffusivity measurements. This reduction in radiation losses was one of Parker's main motivations in developing the flash method[20].

Conclusions

As stated in the introduction, the objectives of this LDRD project were to:

• develop improved processing for HfB_2 - and ZrB_2 - based UHTCs
• create a database of reliable UHTC physical and mechanical properties
• determine the relation between UHTC microstructures and properties using advanced electron microscopic analysis
• determine the origin and type of failure for UHTCs subjected to realistic stresses and feed back that information to improve processing

The results presented above show that we accomplished these goals. We developed a hot pressing technique that reproducibly produced 3 in. diameter, 400 g billets of the Zr and Hf diboride UHTCs. We made the first reported, high quality diboride UHTCs with SiC contents as low as 2%. We used those specimens to measure fracture toughness, 4 point fracture strengths to 1450°C, and thermal diffusivity, thermal expansion, and specific heat up to 2000°C. These measurements have produced high quality data on mechanical and thermal properties as a function of temperature for a wide range of diboride UHTCs.

Use of automated x-ray spectral image analysis (AXSIA) allowed us to determine compositions of small, thin impurity phases on the grain boundaries at a scale never before possible. Those results suggest that the high temperature properties of the UHTCs can be further improved through use of higher purity starting powders and by taking care not to add impurities during processing.

An unresolved scientific question is the densification mechanism for ZrB_2 and HfB_2 and what role the SiC plays in facilitating densification. As discussed above, adding as little as 2 vol% SiC to either HfB_2 or ZrB_2 greatly improves sintering behavior. The theoretical densities increase from 68-75% to nearly 100% under the same processing conditions. The AXISA analysis indicates that a glassy phase is present between the grains in composites containing SiC. This may originate from impurities in the powders or from milling, but other factors may be present as well. Further work to elucidate the sintering mechanism could lead to techniques for pressureless sintering of the diboride UHTCs, which would greatly expand shape making capability and lower processing costs.

REFERENCES

1. Campbell I.E. and Sherwood E. M. (Eds.), "High-Temperature Materials and Technology", Wiley, New York, 1967.

2. Clougherty, E.V., Kaufman, L. "Investigation of Boride Compounds for Very High Temperature Applications," ManLabs, Inc., Cambridge, MA, Air Force Technical Documentary Report No. RTD-TDR-63-4096, 1963.

3. Levine, S.R., et al. "Evaluation of Ultra-High Temperature Ceramics for Aeropropulsion Use," Journal of the European Ceramic Society, vol. 22, no. 14-15, 2002, p. 2757-67.

4. Fahrenholtz, William G. and Gregory E. Hilmas, organizers. "Draft: NSF-AFOSR Joint Workshop on Future Ultra-High Temperature Materials," National Science Foundation Workshop, Arlington, VA, 13-14 January 2004. http://web.umr.edu/~uhtm/

5. Upadhya, K, Jenn-Ming, Y and Wesley P. H, "Materials for Ultrahigh Temperature Structural Applications", the American Ceramic Society Bulletin, December 1997.

6. Monteverde, F., Bellosi A. "Oxidation of ZrB_2-Based Ceramics in Dry Air," Journal of the Electrochemical Society, vol. 150, no. 11, 2003, p. B552-B559.

7. Thermal Properties Research Center (TPRC), Thermophysical Properties of Matter, New York: IFI/Plenum, 1979.

8. Berkowitz-Mattuck, Joan, "High-Temperature Oxidation, Part III. Zirconium and Hafnium Diborides", Journal of the Electrochemical Society, 908-914, 113, No. 9, September 1966.

9. Zheng, Guo-jun, Zhen-Yan D, Naoki K, Jian-Feng Y, and Tatsuki O, "Reactive Hot Pressing of ZrB_2-SiC composites", Journal of American Ceramic Society, 83 [27] 2330-32 (2000).

10. Zheng, Shuqi, Guanghui M, Zengda Z, Huashun Y, Jiande H, and Weiti W, "Oxidation behavior of ZrB_2 powders below 1073 K in air", Metallofizika I Noveishie Tekhnologii, 381-387, 24 (#3) March, 2002.

11. Metcalfe A. G., Elsner N. B., Allen D. T., Hi-Z Technology, Inc., San Diego, California, U.S.A., and E. Wuchina, M. Opeka, Naval Surface Warfare Center, Carderock Division, West Bethesda, Maryland, U.S.A., and E. Opila, NASA Glenn Research Center, Cleveland, Ohio, U.S.A, "Oxidation of Hafnium Diboride", 196th Meeting of the Electrochemical Society, 17 - 22 Oct. 1999, Honolulu.

12. Choy, T.C. Effective Medium Theory: Principles and Applications, Oxford University Press, 1999.

13. Taylor, R.E. "Heat-Pulse Thermal Diffusivity Measurements." High Temperatures – High Pressures, vol. 11, 1979, p 43-58.

14. Tripp, W.C., Davis, H.H., Graham, H.C. "Effect of a SiC Addition on the Oxidation of ZrB_2," American Ceramic Society Bulletin, vol. 52, no.8, 1973, p. 612-616.

15. NIH: ImageJ, Image Processing and Analysis in Java. http://rsb.info.nih.gov/ij (2004).

16. Meyerson, G. A., Samsonov, G. V., Kotel`nikov, R.B., Voyonova, M.S., Yerterjera, I. P., and Krasnenkova, S.D., "Some Properties of Alloys of the Borides of the Refractory Metals of the Transition Groups", Russian Journal of Inorganic Chemistry, Vol. 3, No. 4, pp. 92 - 101, 1958.

17. Kauffman, Larry and Claugherty, Edward, "Investigation of boride compounds for very high temperature applications", Technical documentary report No. RTD-TDR-63-4096, Part II, Manlabs, Inc., December 1964.

18. ASTM E 1461-01, "Standard Test Method for Thermal Diffusivity by the Flash Method," ASTM International.

19. NBS Special Publication 260-89, "Standard Reference Materials: A Fine-Grained, Isotropic Graphite for Use as NBS Thermophysical Property RM's from 5 to 2500 K," U.S. Department of Commerce, National Bureau of Standards, 1984.

20. Parker, W.J. et al. "Flash Method of Determining Thermal Diffusivity, Heat Capacity, and Thermal Conductivity." Journal of Applied Physics, V. 12, n. 9, 1961. p. 1679-1685.

21. Heckman, R.C. Journal of Applied Physics, vol. 44, 1973, p. 1455.

22. Cowan, R.D. Journal of Applied Physics, vol. 34, 1963, p. 926.

23. Clark III, L.M., Taylor, R.E. "Radiation Loss in the Flash Method for Measurement of Thermal Diffusivity," Journal of Applied Physics, vol. 46, no. 2, 1975, p. 714-718.

24. Thermitus, M., "Thermal Diffusivity and Flash Method," Anter Corporation, White paper. Pittsburg. No date.

25. McCluskey, P.H., et al. "Thermal Diffusivity/Conductivity of Alumina-Silicon Carbide Composites," Journal of the American Ceramic Society, vol. 73, no. 2, 1990, p. 461-4.

26. McKelvey, John P. Solid State and Semiconductor Physics. New York: Harper and Row, 1966.

27. ASTM E 1269-99, "Standard Test Method for Determining Specific Heat Capacity by Differential Scanning Calorimetry," ASTM International.

28. ASTM E 968-99, "Practice for Heat Flow Calibration of Differential Scanning Calorimeters," ASTM International.

29. Joshi, R.P., Neudeck, P.G., Fazi, C. "Analysis of the Temperature Dependent Thermal Conductivity of Silicon Carbide for High Temperature Applications," Journal of Applied Physics, vol. 88, no. 1, 2000, p. 265-69.

See also NIST. NIST Property Data Summaries for Sintered Silicon Carbide (SiC), http://www.ceramics.nist.gov/srd/summary/scdscs.htm, 8 February 2001.

36. Anna E. McHale, "Phase Equilibrium Diagrams – Phase Diagrams for Ceramists", National Institute of Standards and Technology, Volume X, The American Ceramic Society, 131&145, 1994.

37. A. K. Kuriakose and J. L. Margrave, "The Oxidation Kinetics of Zirconium Diboride and Zirconium Carbide at High Temperatures", Journal of the Electrochemical Society, Vol. 111, No. 7, 827-31, 1964.

38. W. C. Tripp and H. C. Graham, "Thermogravimetric Study of the Oxidation of ZrB_2 in the temperature range of 800^0 to 1500^0C", Journal of Electrochemical Society, Vol. 118, No. 7, 1195-99, 1971.

39. C. Brent Bargeron, Richard C. Benson, Robb W. Newman, A. Norman Jette, and Terry E. Phillips, "Oxidation mechanisms of Hafnium Carbide and Hafnium Diboride in the Temperature Range 1400 to 2100^0C", John Hopkins APL Technical Digest, Vol. 14, No. 1, 29-36, 1993.

40. Alan W. Weimer, "Carbide, Nitride and Boride Materials Synthesis and Processing", Chapman & Hall, London, 1997.

41. E. Rudy and J. Progulski, "A Pirani Furnace for the Precision Determination of the Melting Temperatures of Refractory Metallic Substances", Planseeberichte für Pulvermetallurgie, Vol. 15, pp 13-45, 1967.

42. G. A. Meyerson and O. E. Krein, "The Preparation of Hafnium Carbide", Russian Journal of Inorganic Chemistry, Vol. 5, No. 5, pp 559-61, May 1960.

DISTRIBUTION

UNLIMITED RELEASE

<u>Copies</u>

MS1349	10	R. E. Loehman, 1815
MS1349	1	Erica Corral, 1815
MS 0886	1	Paul Kotula, 1822
MS 0886	1	Ray Goehner, 1822
MS 1411	1	Rajan Tandon, 1825
MS 0889	1	Jeff Braithwaite, 1825
MS 1349	1	W. F. Hammetter, 1815
MS 0887	1	J. Johannes, 1810
MS 0887	1	D. B. Dimos, 1800
MS 0384	1	Art Ratzel, 1500
MS 0825	1	Basil Hassan, 1515
MS 0825	1	David Kuntz, 1515
MS 1162	1	Walt Rutledge, 5422
MS 1164	1	John Macha, 5422
MS 1164	1	Eric Schindwolf, 5420
MS 0188	1	LDRD Office, Org. 4001
MS 0123	1	Donna Chavez, LDRD Office, Org. 1011
MS 9018	2	Central Technical Files, Org. 8945-1
MS 0899	2	Technical Library, Org. 4536